



INSTITUT DE FRANCE
Académie des sciences

Comptes Rendus

Géoscience

Sciences de la Planète

Zineb Nabyl, Fabrice Gaillard, Johann Tuduri and Ida Di Carlo

No direct effect of F, Cl and P on REE partitioning between carbonate and alkaline silicate melts


Volume 353, issue S2 (2021), p. 233-272

<https://doi.org/10.5802/crgeos.104>

Part of the Special Issue: Perspectives on alkaline magmas

Guest editor: Bruno Scaillet (Institut des Sciences de la Terre d'Orléans, CNRS, France)

© Académie des sciences, Paris and the authors, 2021.
Some rights reserved.

 This article is licensed under the
CREATIVE COMMONS ATTRIBUTION 4.0 INTERNATIONAL LICENSE.
<http://creativecommons.org/licenses/by/4.0/>



*Les Comptes Rendus. Géoscience — Sciences de la Planète sont membres du
Centre Mersenne pour l'édition scientifique ouverte
www.centre-mersenne.org*



Perspectives on alkaline magmas / *Perspectives sur les magmas alcalins*

No direct effect of F, Cl and P on REE partitioning between carbonate and alkaline silicate melts

Zineb Nabyl^{*, a}, Fabrice Gaillard^a, Johann Tuduri^{a, b} and Ida Di Carlo^a

^a ISTO, UMR 7327, Université d'Orléans, CNRS, BRGM, F-45071 Orléans, France

^b BRGM, F-45060 Orléans, France

E-mails: zineb.nabyl@gmail.com (Z. Nabyl), fabrice.gaillard@cnrs-orleans.fr (F. Gaillard), j.tuduri@brgm.fr (J. Tuduri), ida.di-carlo@cnrs-orleans.fr (I. D. Carlo)

Abstract. This study presents new insights into the effects of halogens (F and Cl) and phosphorous (P) on rare earth element (REE) partitioning between carbonatite and alkaline silicate melts. F, Cl and P are elements that are abundant in carbonatites and alkaline magmatic systems and they are considered to play an important role on the REE behaviour. Nonetheless, their effect on REE partitioning between carbonate and alkaline silicate melts has not yet been constrained.

Here we present new experimental data on REE partitioning between carbonate and alkaline silicate melts doped in F, Cl and P, in order to (1) test the Nabyl et al. [2020] REE partitioning model in F-, Cl- and P-rich systems, and (2) identify the possible role of F, Cl and P in carbonate melt REE enrichments during alkaline-carbonatite magma differentiation. The experiments were performed at 850–1050 °C and 0.8 GPa using piston-cylinder devices. Starting materials consisted of carbonatite and phonolite compositions \pm doped in F, Cl and P. The experimental results show that REE partitioning is similar in F-Cl-P-rich and -poor systems. The silicate melt composition and its molecular structure (i.e. SiO₂ contents, the alumina saturation index and the alkali/alkaline-earth element ratio), which have already been identified as controlling REE partitioning in F-, Cl- and P-poor systems, still operate in doped systems. No direct effect of the F, Cl or P melt concentrations on REE partitioning has been identified. We also propose an application to natural systems.

Keywords. Carbonatites, Alkaline magma, Halogens, Phosphorous, Rare earth elements, Immiscibility processes.

1. Introduction

Carbonatites and alkaline magmatic rocks are known to be the most REE enriched igneous rocks [Nelson et al., 1988, Woolley and Kempe, 1989] and are associated with the most important REE deposits [Chakhmouradian and Zaitsev, 2012, Smith et al., 2016, Verplanck et al., 2016]. These rocks are also enriched in volatile species such as halogens—fluorine

and chlorine (F and Cl)—[Aiuppa et al., 2009, Jago and Gittins, 1991, Jones et al., 2013, Kynicky et al., 2019, Metrich and Rutherford, 1992, Webster et al., 2018], and also phosphorous [Ablay et al., 1998, Jones et al., 2013, Mattsson et al., 2013, Woolley and Kempe, 1989]. These elements can reach more than 1 weight % (wt%) in alkaline silicate magmatic rocks [Ablay et al., 1998, Aiuppa et al., 2009, Baudouin et al., 2016, Mangler et al., 2014, Mattsson et al., 2013, Webster et al., 2018]. F, Cl and P concentrations are also high in carbonatites [Jones et al., 2013, Woolley and Kempe, 1989], especially in the

* Corresponding author.

natrocarbonatites—the alkali-rich carbonatite lavas from the Ol Doinyo Lengai volcano in Tanzania—in which concentrations can reach more than 4, 3 and 1 wt% respectively [Dawson, 1962, Keller and Zaitsev, 2012]. These elements are also found in minerals present in carbonatites and alkaline magmatic rocks and constitute major components of important REE mineral phases [Verplanck *et al.*, 2016]. In fact, the REE are mostly contained in fluoro-carbonates such as bastnaesite and synchisite, or in phosphates such as monazite and apatite [Smith *et al.*, 2016, Verplanck *et al.*, 2016]. The REE mineralisation is frequently described as resulting from late- to post-magmatic processes involving fluid circulation, which are often characterised as F-, Cl- and P-rich [Gysi and Williams-Jones, 2015, Smith *et al.*, 2016, Verplanck *et al.*, 2016, Williams-Jones *et al.*, 2012]. These elements play an important role in the concentration, redistribution and deposition processes of REE [Jia and Liu, 2020, Louvel *et al.*, 2015, Migdisov *et al.*, 2016, Williams-Jones *et al.*, 2012]. Nonetheless, primary monazite or bastnaesite crystals have also been recognised and defined as magmatic phases in carbonatites [Castor, 2008, Feng *et al.*, 2020, Mariano and Mariano, 2012, Néron *et al.*, 2018, Verplanck *et al.*, 2016, Wall and Mariano, 1996]. The REE mineralisation can therefore originate from both magmatic or hydrothermal processes, and the boundary between the two mechanisms remains unclear [Anenburg *et al.*, 2020, Chakhmouradian and Zaitsev, 2012, Verplanck *et al.*, 2016].

Salt-rich melts (including F-, Cl-, P- and S-rich melts) formed at the magmatic stage have been directly demonstrated by the study of natrocarbonatites enriched in F, Cl, P and SO₃ [Dawson, 1962, Keller and Zaitsev, 2012, Mangler *et al.*, 2014, Potter *et al.*, 2017]. Melt inclusion studies have also highlighted the existence of salt melts coexisting with silicate melts [Feng *et al.*, 2020, Frezzotti, 2001, Panina, 2005, Panina and Motorina, 2008], and especially F-, Cl- and P-rich immiscible alkaline silicate and carbonate melts [Berkesi *et al.*, 2020, Guzmics *et al.*, 2019]. Such occurrences, combined with the fact that the most important REE-minerals in carbonatites correspond to fluoro-carbonates and phosphates, raise the question as to whether there is a link between F, Cl and P and the behaviour of REE in conjugate carbonate and silicate melts.

Here we focus on the immiscibility processes be-

tween carbonate and silicate melts. This is motivated by the strong association of carbonatites and alkaline silicate rocks observed in the field [Kjarsgaard and Hamilton, 1988, Mitchell, 2005, Woolley and Kjarsgaard, 2008], by melt inclusion studies of conjugate carbonate and silicate melts, as mentioned above [Baudouin *et al.*, 2018, Berkesi *et al.*, 2020, Guzmics *et al.*, 2012, 2019, Mitchell, 2009], and also by experimental investigations simulating the immiscibility between carbonate and silicate melts [Brooker, 1998, Brooker and Kjarsgaard, 2011, Hamilton *et al.*, 1989, Lee and Wyllie, 1994, Martin *et al.*, 2012, 2013, Massuyeau *et al.*, 2015, Nabyl *et al.*, 2020, Veksler *et al.*, 1998, 2012]. Experimental studies on trace element partitioning between carbonate and silicate melts [Hamilton *et al.*, 1989, Martin *et al.*, 2013, Nabyl *et al.*, 2020, Veksler *et al.*, 1998, 2012] have shown that carbonate melt immiscible with silicate melt can either be strongly depleted or, on the contrary, enriched in REE. This large variation has been linked by Nabyl *et al.* [2020] to the silicate melt composition and structure. Nabyl *et al.* [2020] have proposed a modelling of carbonatite REE enrichment along the alkaline magma differentiation course which is exclusively based on the silicate melt composition. This model allows the REE composition of a carbonate melt immiscible with a silicate melt to be calculated from parameters relative to the silicate melt composition: the silica content (SiO₂), the alumina saturation index (Al₂O₃/(CaO + Na₂O + K₂O)) and the alkali/alkaline-earth cation ratio [(Na₂O + K₂O)/(CaO + MgO); Nabyl *et al.*, 2020]. Using this model, Nabyl *et al.* [2020] have shown that REE-rich carbonate melts can be immiscible with highly differentiated and polymerised alkaline silicate melts of phonolitic/phonotrachytic type, and hence that the degree of silicate melt differentiation plays a key role in the conjugate carbonate melt REE enrichment. The parameterisation of the model has been performed in experimental studies mentioned above [Hamilton *et al.*, 1989, Martin *et al.*, 2013, Nabyl *et al.*, 2020, Veksler *et al.*, 1998, 2012]. However, this model does not take into account the role of F, Cl and P in carbonate melt REE enrichments.

In the pure salt melt (pure fluoride/chloride/phosphate) and silicate melt systems [Chebotarev *et al.*, 2019, Veksler *et al.*, 2005, 2012], experimental studies have broadly shown that REE have a strong affinity for salt melts, with the enrich-

ment varying by two orders of magnitude [Veksler *et al.*, 2012]. Kynicky *et al.* [2019] and Feng *et al.* [2020] have also proposed that carbonate melt salt components (F- and P-rich carbonate melts respectively) can significantly favour REE enrichment. Besides, these elements are critical in the silicate melt structure. Fluorine has been shown to be highly soluble in silicate melts [Dingwell, 1986], creating potential complexes with major elements such as Ca, Na, Si and Al [Baasner *et al.*, 2014, Schaller *et al.*, 1992], or with REE [Ponader and Brown, 1989], and as being involved in the silicate melt polymerisation as well as depolymerisation [Ponader and Brown, 1989], in addition to affecting its viscosity [Baasner *et al.*, 2013a,b]. Baasner *et al.* [2014] have also shown that F can create bonds with network-modifying cations such as Ca and Na in peralkaline silicate melts, whereas it creates complexes with network-building cations such as Si and Al in peraluminous melts. Chlorine has also been described as having an effect on silicate melt viscosity [Baasner *et al.*, 2013b,a]. Several studies have also characterised P as playing a role in the silicate melt structure [Mysen, 1998, Mysen *et al.*, 1981, Toplis and Dingwell, 1996], forming complexes with Ca, Mg, Na and Al [Mysen, 1998, Mysen *et al.*, 1981], and increasing the viscosity of peralkaline silicate melts [Toplis and Dingwell, 1996]. Altogether, this suggests that F, Cl and P can have an effect on the structure of alkaline silicate melt coexisting with carbonate melt, hence influence the REE behaviour between both melts. However, the current experimental database does not allow us to determine the impact of these elements on the REE partitioning between carbonate and silicate melts.

The aim of this study is to test the Nabyl *et al.* [2020] model in F-, Cl- and P-rich environments and to characterise the role of these elements in the REE partitioning between carbonate and alkaline silicate melts. We present high temperature–high pressure experiments simulating the immiscibility between carbonate and alkaline silicate melts of evolved nephelinite–phonolite type, in F-, Cl- and P-rich systems. The experiments were performed at 850–1050 °C and 0.8 GPa. We show that F, Cl and P do not play a direct role in carbonate melt REE enrichment, and that REE partitioning in F-, Cl- and P-rich systems can be predicted using the Nabyl *et al.* [2020] model.

2. Methodology

2.1. Experimental strategy

Four compositions were synthesized (Table 1) with a base composition of a phonolite–carbonatite mixture in a ratio of 50:50 for the major elements (including Si, Ti, Al, Fe, Mn, Mg, Ca, Na, K, P, Ba, Sr, F and Cl). The selected mixture composition corresponds to the immiscible carbonate melt and silicate melt of phonolitic composition from experiment T19_01 of Nabyl *et al.* [2020]. This base composition (composition PhCbn1, see Table 1; named “non-doped” in the following text) contains small amounts of F, Cl and P (F ~ 1 wt%; Cl ~ 0.3 wt%; P₂O₅ ~ 0.7 wt%; Table 1). In order to characterise and isolate a possible volatile effect on the REE partitioning, three compositions were doped with ca. 5 wt% of P₂O₅ (composition PhCbn2, Table 1), F (composition PhCbn3, Table 1) and Cl (composition PhCbn4, Table 1) respectively. All four starting materials also contain 0.1 wt% of Σ REE-Y-Sc and other trace elements (see Table 1).

Most experiments were performed at 850 °C and 0.8 GPa [similar to experiment T19_01 in Nabyl *et al.*, 2020]. Additional experiments were also performed at a higher temperature (1050 °C). Moreover, different amounts of water (0, 3 or 6 wt%) were added to the starting material to test its effect on each chemical system.

2.2. Starting compositions

The four starting compositions (Table 1) were prepared by mixing synthetic powders (SiO₂, TiO₂, Al₂O₃, AlPO₄, AlF₃, AlCl₃, FeO, FeS, MnCO₃, CaCO₃, Na₂CO₃, K₂CO₃, BaCO₃, SrCO₃ and Cr₂O₃) and natural dolomite (CaMg(CO₃)₂). For the three \pm F-, Cl- and P-doped compositions (PhCbn2, PhCbn3 and PhCbn4 respectively, Table 1), additional AlF₃, AlCl₃ and AlPO₄ powders were used to reach the respective F, Cl and P concentrations needed (Table 1). The starting compositions are CO₂-rich, with bulk concentrations of ca. 24 wt%. REE and other trace elements were also added to the four compositions in the form of oxides, fluorides or pure elements (La₂O₃, CeO₂, Pr₆O₁₁, Nd₂O₃, Sm₂O₃, Eu₂O₃, GdF₃, Tb, Dy₂O₃, HoF₃, Er₂O₃, Yb₂O₃, Lu, Y₂O₃, Sc₂O₃, Nb₂O₅, Ta₂O₅, ZrO₂ and HfO₂).

The synthetic powders were maintained in a dry oven at 120 °C, except for the strong hydrophilic

Table 1. Starting material compositions

	PhCbn 1	PhCbn 2	PhCbn 3	PhCbn 4
Major elements in wt%				
SiO ₂	25.47	24.32	24.37	24.01
TiO ₂	0.34	0.32	0.32	0.31
Cr ₂ O ₃	0.01	0.01	0.01	0.01
Al ₂ O ₃	9.47	9.36	8.95	8.88
Fe ₂ O ₃	3.88	3.67	3.7	3.52
MnO	0.31	0.29	0.29	0.28
MgO	1.06	1	0.98	0.97
CaO	14.88	14.16	14.25	13.65
Na ₂ O	12.19	11.51	11.5	11.07
K ₂ O	4.01	3.95	3.7	3.54
P ₂ O ₅	0.76	5.13	0.76	0.71
SrO	0.77	0.7	0.68	0.66
BaO	0.56	0.54	0.54	0.54
F	1.12	1.03	5.83*	1.03
Cl	0.34	0.34	0.28	4.72*
S	0.06	0.06	0.06	0.05
LOI	24.77	23.72	23.78	26.07
Total	100	100	100	100
Trace elements in µg/g (ppm)				
Ba	5340	5080	5370	5410
Sr	7000	6450	6380	6120
Hf	23.4	22.5	17.9	24.4
Zr	407	379	371	377
Nb	197	198	185	163.5
Ta	12.4	9.7	4.4	6
La	52.5	50.9	49.8	48.9
Ce	61	59.6	60.4	56.6
Pr	51	51.4	49.4	47.2
Nd	53.6	53.6	51	50.2
Sm	56.1	55.8	54.3	50.1
Eu	55	55.7	53.9	52.5
Gd	61.5	55.3	56.6	55.4
Tb	52.4	50.7	52.1	50.1
Dy	57.3	56.8	56.5	56.7
Ho	52.6	53.3	54.2	52.5
Er	57.7	57.2	58.8	58.5
Yb	54.9	55.3	56	54.6
Lu	49.9	49.7	49.9	48.3

(continued)

Table 1. (continued)

	PhCbn 1	PhCbn 2	PhCbn 3	PhCbn 4
Y	67.4	67.7	64.9	63.5
Sc	64	58	56	60
Cr	140	120	120	120

Major elements (wt%) and trace elements (µg/g, ppm) were analysed by ICP-MS analysis on powders (ALS Global); *: concentrations calculated on a normalised basis. Experimental conditions and run products. *P*: total pressure; *T*: temperature; SL: silicate liquid; CL: carbonate liquid; CPx: clinopyroxene (diopside–hedenbergite–wollastonite solution); Nph: nepheline; Gnt: garnet (andradite); Ap: apatite; Fe-Spl: iron-spinel (magnetite–titanomagnetite solid solution); Spl: spinel; Afs: alkali feldspar; Cal: calcite; Fl: fluorite; Fst: feldspathoid; “CL2”: second carbonate liquid phase; V: vapour phase.

Na₂CO₃ and K₂CO₃ powders which were preserved in an oven at 200 °C. Moreover, the AlF₃, AlCl₃ and AlPO₄ powders were also strongly hydrophilic at atmospheric conditions and could not be preserved at temperatures higher than 50 °C. Those powders and both the PhCbn3 and PhCbn4 compositions (Table 1) were thus manipulated using a Captair Pyramid 2200 ANM-XLS at controlled atmosphere under Argon gas to avoid any atmospheric water contamination, and maintained in a vacuum bell jar. For each composition, the powders were first mixed by hand in an agate mortar (30 min) and then in an automatic grinder with an agate mortar and ball mill (at least two times for 15 min).

2.3. Piston-cylinder experiments

We synthesized 20 experimental charges at 0.8 GPa, 850 and 1050 °C using an end-loaded piston-cylinder apparatus (Table 2). The starting materials were packed into Au capsules (diameter of 2.5–2.9 mm) for low temperature experiments (850 °C) and Au₈₀Pd₂₀ capsules for higher temperature ones (1050 °C). For experiments performed at 850 °C and 0.8 GPa and for almost all the starting materials, four capsules were

synthesized: one capsule containing only the starting material, two capsules containing 3 and 6 wt% of water respectively (Table 2), and one capsule with additional graphite (+1 wt%, see Table 2). Water and graphite were added in order to test their effect on carbonate and silicate melt compositions.

The capsules were introduced into an alumina tube with a powder composed of 50% AlSiMag (mixture of Al, Si and Mg)–50% haematite, and closed at the top and bottom with MgO-plugs. The fO_2 for the experiments was estimated at between FMQ and FMQ+2, due to the presence of the haematite powder which creates an oxidised environment (i.e. H_2 -poor). Graphite-bearing experiments were more reduced, likely in the range FMQ–2 [Stagno and Frost, 2010]. The whole assemblage was packed into a 3/4-inch piston-cylinder assembly, composed of graphite, pyrex and talc. Two steel-plugs surrounded by pyrophyllite were placed at the top and bottom of the assembly to maintain the assemblage in place; the thermocouple (B-type, Pt₉₄Rh₆–Pt₇₀Rh₃₀) was introduced in the top of the assemblage. For the experiments conducted at 850 °C (Table 2), the samples were first taken up to 975 °C for two hours to ensure bulk composition melting and homogenisation, then the final temperature (850 °C) was reached within a few minutes (cooling rate of 10 °C per minute). Each experiment was quenched by switching off the heat source at isobaric conditions. Uncertainties for the temperature and the pressure are considered to be ± 12 °C and ± 0.1 GPa respectively [Dasgupta *et al.*, 2004, Sifré *et al.*, 2014].

2.4. Analytical methods

Polished sections were prepared from the experimental charges, and observed using a Merlin Compact Zeiss electron microscope (voltage 15 kV), equipped with a micro-analyser system EDS (Bruker-QUANTAX-XFlash6, resolution 129 eV) at the ISTO laboratory, in order to determine the phases and their textures. Carbonate and silicate melt sections were then analysed with a Cameca SXFive electron microprobe equipped with 5 WDS detectors (ISTO, France) at 15 kV and 6 nA. Analyses were performed with a large beam size (from 10 to 70 μm) to avoid any Na-loss and to average carbonate melt compositions. The standards used for the calibration were

albite, apatite, orthose, andradite, topaz, vanadinite, MgO, Al_2O_3 , Fe_2O_3 , $MnTiO_3$, $BaSO_4$, and $SrCO_3$. The counting time was 10 s for all the elements, except for Ba (20 s), Sr and Nb (30 s) and S (60 s). Higher counting times were also needed for F, Cl and P to ensure representative analyses (30 s for Cl, 60 s for F, and 60 or 120 s for P).

Trace elements were analysed using two different LA-ICP-MS (Laser Ablation Inductively Coupled Plasma Mass Spectrometry) devices: the Agilent 7500 CS Quadrupole ICP-MS of the LMV laboratory (Clermont-Ferrand, France; He: 550 mL/min; Ar: 850 mL/min; N_2 : 2 mL/min) and the Agilent 7900 Quadrupole ICP-MS of the ISTO laboratory (Orléans, France; He: 350 mL/min; Ar: 930 mL/min). Both mass spectrometers are coupled to a 193 nm excimer laser ablation system (Resonetics), with He flushing the ablation cell. Carbonate and silicate melt analyses were performed with a frequency of 2 Hz, an ablation energy of 1.5–3 mJ and a beam size of 14 to 60 μm in diameter, depending on both melt/crystal-free areas. Carbonate and silicate melts from several samples were analysed with both spectrometers to ensure similar trace element concentrations were obtained and that no bias was induced by using the two different machines. The following isotopes were analysed: ^{43}Ca , ^{44}Ca , ^{29}Si , ^{139}La , ^{140}Ce , ^{141}Pr , ^{146}Nd , ^{147}Sm , ^{153}Eu , ^{157}Gd , ^{159}Tb , ^{163}Dy , ^{165}Ho , ^{166}Er , ^{172}Yb , ^{175}Lu , ^{89}Y , ^{45}Sc , ^{49}Ti , ^{53}Cr , ^{55}Mn , ^{88}Sr , ^{137}Ba , ^{93}Nb , ^{181}Ta , ^{90}Zr , ^{178}Hf , ^{197}Au and ^{105}Pd to verify any potential contamination by the capsule during the experiment.

Data reduction and trace element concentrations were carried out using the GLITTER4.4 software [Van Acherbergh *et al.*, 2001] for both the carbonate and silicate melts. The elements were quantified using the NIST 610 standard glass [Pearce *et al.*, 1997] and other standards were used to check the analysis validity [NIST 612 and BCR-2G natural basaltic glass; Pearce *et al.*, 1997, Rocholl, 1998, Jochum *et al.*, 2016]. The standards were analysed at the same beam size, frequency and energy ablation as the samples to verify the efficiency of the analysis. The Ca was used as the internal standard, its concentration having first been determined by electron microprobe analyses in both the carbonate and the silicate phases.

Table 2. Experimental conditions and run products

Experiment	Starting material	Added volatile	P (GPa)	T (°C)	Duration (h)	Capsule material	Added water (wt%)	Added graphite (wt%)	Phases
PCPC1_01	PhCbn1	—	0.8	850	50	Au	—	—	SL + CL + CPx + Nph + Gnt + Spl + Fe-Spl + V (+“CL2”)
PCPC1_02	PhCbn1	—	0.8	850	50	Au	3	—	SL + CL + CPx + Nph + Gnt + Fe-Spl + V (+“CL2”)
PCPC1_03	PhCbn1	—	0.8	850	50	Au	6	—	SL + CL + Fe-Spl + V
PCPC1_04	PhCbn1	—	0.8	850	50	Au	—	1	CL + Cpx + Nph + Gnt + Afs
PCPC2_01	PhCbn1	—	0.8	1050	28	Au ₈₀ Pd ₂₀	—	—	SL + CL + Nph
PCPC3_01	PhCbn2	P	0.8	850	67.5	Au	—	—	SL + CL + Nph + Ap + Spl + Fe-Spl
PCPC3_02	PhCbn2	P	0.8	850	67.5	Au	3	—	SL + CL + Ap + Spl + Fe-Spl
PCPC3_03	PhCbn2	P	0.8	850	67.5	Au	6	—	SL + CL + Ap + Fe-Spl
PCPC3_04	PhCbn2	P	0.8	850	67.5	Au	—	1	CL + Cpx + Nph + Gnt + Ap + Fe-Spl + Afs
PCPC4_01	PhCbn3	F	0.8	850	88.5	Au	—	—	SL + CL + Fl + Cal + Fe-Spl
PCPC4_02	PhCbn3	F	0.8	850	88.5	Au	3	—	SL + CL + Fl + Cal + Fe-Spl
PCPC4_03	PhCbn3	F	0.8	850	88.5	Au	6	—	SL + CL + Fl + Cal + Fe-Spl
PCPC4_04	PhCbn3	F	0.8	850	88.5	Au	—	1	CL + Fl + Cpx + Nph + Gnt + Fl + Spl + Fe-Spl + Afs + Fst
PCPC5_02	PhCbn4	Cl	0.8	850	88.5	Au	3	—	SL + CL + CPx + Gnt + Ap + Cal + V
PCPC5_03	PhCbn4	Cl	0.8	850	88.5	Au	6	—	SL + CL + CPx + Gnt + Ap + V
PCPC5_04	PhCbn4	Cl	0.8	850	88.5	Au	—	1	CL + Cpx + Nph + Gnt + Ap + Cal + Afs + Fst
PCPC6_01	PhCbn3	F	0.8	1050	23.5	Au ₈₀ Pd ₂₀	—	—	SL + CL
PCPC6_02	PhCbn4	Cl	0.8	1050	23.5	Au ₈₀ Pd ₂₀	—	—	SL + CL
PCPC6_03	PhCbn2	P	0.8	1050	23.5	Au ₈₀ Pd ₂₀	—	—	SL + CL + Ap

P: total pressure; T: temperature; SL: silicate liquid; CL: carbonate liquid; CPx: clinopyroxene (diopside–hedenbergite–wollastonite solution); Nph: nepheline; Gnt: garnet (andradite); Ap: apatite; Fe-Spl: iron-spinel (magnetite–titanomagnetite solid solution); Spl: spinel; Afs: alkali feldspar; Cal: calcite; Fl: fluorite; Fst: feldspathoid; “CL2”: second carbonate liquid phase; V: vapour phase.

3. Results

3.1. Carbonate and silicate melt textures

Nineteen samples were synthesized at 0.8 GPa and 850 and 1050 °C. For the sake of clarity, each chemical system is represented with a different colour in all the figures: black for the non-doped system, red for the P-rich system, green for the Cl-rich system and blue for the F-rich system.

For all starting materials (\pm F, Cl and P), all run products have an alkaline silicate liquid conjugated with a carbonate liquid, apart from those produced at 850 °C with graphite (samples noticed "..._04", see Table 2) which have only a carbonate melt coexisting with a few silicate crystals. The silicate liquids quenched into homogeneous glass in all the samples (Figures 1 and 2). The coexisting carbonate melts show typical textures of quenched crystallised dendritic blebs in almost all the systems (non-doped system, P- and Cl-rich system; Figures 1 and 2), the exception being the F-rich system where they have a near-glassy texture (Figures 1c, 2e and f). In the Cl-rich system (Figures 1d and 2g), carbonate blebs display a porous texture. For almost all the samples, the clear contact between both liquids, the homogeneous chemical compositions and the size of the carbonate melts (up to 200 μ m) indicate that equilibrium has been attained between both liquids at given P–T conditions, and this attests to the fact that immiscibility is not related to quench processes [Brooker and Kjarsgaard, 2011]. In two samples from the non-doped system that were synthesized at 850 °C (PCPC1_01 and PCPC1_02, Figures 2a and b; Table 2), a second distinct carbonate liquid phase is observed (noted "CL2", in Figure 2b), characterised by carbonate blebs of <15 to 50 μ m. This phase will be treated separately in the following section of the results.

In some samples (Table 2), bubbles are observed (Figure 1d; Figures 2d and f) and attest to the presence of a fluid phase coexisting with both liquids. Moreover, at 0.8 GPa and 1050 °C carbonate melts contain a large amount of apatite crystals in the P-rich sample (Figure 1b), while no apatite are observed in the F- and Cl-rich systems (Figures 1c and d respectively). At the lower temperature (850 °C), all charges contain crystals (Figure 2 and Table 2). Clinopyroxene is mainly present in non-doped samples (Figures 2a and b) and in Cl-rich samples (in

green, Figure 2g). Apatite is also present in significant proportions in the carbonate melt zones of P-rich samples (Figures 2c and d; Table 2), and a few apatite crystals are also observed in the Cl-rich samples (Figure 2g, Table 2). Other phases are also observed, such as nepheline, garnet, spinel, alkali feldspar, feldspathoid, calcite and fluorite (Table 2, see Figure 2). The chemical composition of all minerals is not discussed here as this study is mainly focused on the effect of F, Cl and P on REE partitioning between the carbonate and alkaline silicate melts.

3.2. Chemical composition of the melts

The major element concentrations of the conjugate silicate and carbonate melts are presented in Table 3.

At 0.8 GPa and 1050 °C for all four chemical systems, the silicate melts present a composition of alkaline nephelinite type, with the SiO₂ content varying slightly from 42.9 \pm 0.2 wt% (sample PCPC6_02 in the Cl-rich system, Table 3) to 46.3 \pm 0.6 wt% (sample PCPC6_03 in the P-rich system, Table 3), and alkali contents (Na₂O + K₂O) from 15.1 \pm 0.8 wt% (sample PCPC6_02 in the Cl-rich system, Table 3) to 17.8 \pm 0.6 wt% (sample PCPC6_01 in the non-doped system, Table 3). Figure 3 presents ternary diagrams in the Hamilton projection—i.e. in the (Na₂O + K₂O)–(SiO₂ + TiO₂ + Al₂O₃)–(CaO + MgO + FeO) space—which is widely used to represent the miscibility gap between carbonate and silicate melts [Freestone and Hamilton, 1980, Kjarsgaard and Hamilton, 1988]. The silicate melts in the P- and F-rich systems are slightly richer in silica and alkali elements compared to those in the non-doped and Cl-rich systems (Figure 3a, see Table 3). The conjugate carbonate melt compositions vary in the four chemical systems from 10.1 \pm 1.6 to 17.1 \pm 0.7 wt% Na₂O (samples PCPC6_02 and PCPC6_03 respectively, Table 3) and from 29.4 \pm 0.9 to 34.3 \pm 1.2 wt% CaO (samples PCPC6_03 and PCPC2_01, respectively, Table 3). The carbonate melts of the Cl-rich system are poorer in Na₂O content compared to the others, and thus closer to the (CaO + MgO + FeO) pole (Figure 3a).

The F, Cl and P₂O₅ silicate melt concentrations at 1050 °C for all the systems are relatively high, reaching almost 4, 1.3 and 1 wt% in the F-, Cl- and P-rich systems respectively (Table 3). In the carbonate

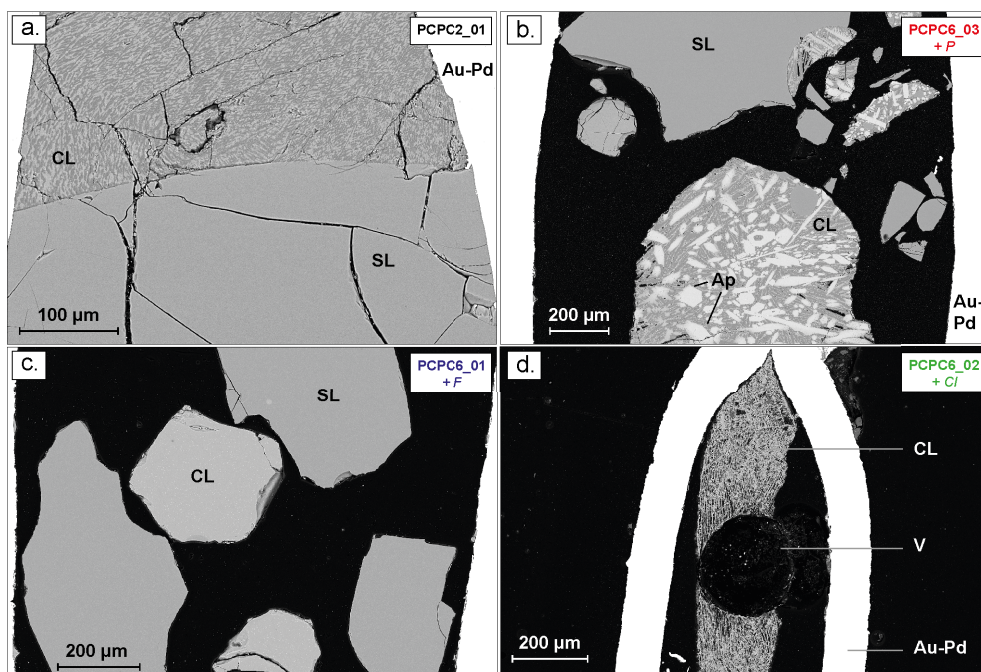


Figure 1. BSE images of typical experimental carbonate and silicate liquid immiscibility at 1050 °C and 0.8 GPa, in the non-doped system in black (a), in the P-rich system in red (b); in the F-rich system in blue (c) and in the Cl-rich system in green (d). SL: silicate liquid; CL: carbonate liquid; Ap: apatite; V: fluid phase; Au-Pd: gold–palladium capsule.

melts, F and P_2O_5 concentrations are much higher in the F- and P-rich systems: F reaches 11.8 ± 0.7 wt% in the F-rich system (sample PCPC6_01, Table 3), and the carbonate melt in the P-rich system contains 9.5 ± 0.9 wt% P_2O_5 (sample PCPC6_03, Table 3). However, in the Cl-rich system for the carbonate melt the Cl concentration remains low (0.9 ± 0.3 wt%, sample PCPC6_02, Table 3).

At the lower temperature (850 °C, Figure 3b and Table 2), partial crystallisation changes the silicate melt composition from evolved nephelinite to phonolite type, i.e. from 45.8 ± 0.9 to 53.7 ± 0.8 wt% SiO_2 (samples PCPC5_03 and PCPC4_01 respectively, Table 3) and 16.2 ± 0.6 to 18.0 ± 0.5 wt% $Na_2O + K_2O$ (samples PCPC5_03 and PCPC3_03 respectively, Table 3). For all four chemical systems, the miscibility gap between the carbonate and silicate melts is enlarged as temperature decreases from 1050 to 850 °C (Figures 3a and b), with silicate melts getting closer to the ($SiO_2 + TiO_2 + Al_2O_3$) pole and carbonate melts getting closer to

the ($CaO + MgO + FeO$) pole. Silicate melts present similar compositions for all the chemical systems (Figure 3b; Table 3) and for samples \pm hydrated (dashed and dotted lines, 3 and 6 wt% of H_2O respectively, Figure 3b). In contrast, the conjugate carbonate melts vary significantly in the four chemical systems. Carbonate melts are broadly richer in CaO with concentrations varying from 31.0 ± 1.4 to 36.8 ± 5.1 wt% (samples PCPC1_03 and PCPC5_03 respectively, see Table 3), except for the P-rich system, which shows lower CaO concentrations, between 24.4 ± 1.8 and 25.4 ± 2.8 wt% (samples PCPC3_01 and PCPC3_02, Table 3). Carbonate melts are also slightly richer in Na_2O in the non-doped system and in the F- and P-rich systems, with concentrations varying from 14.7 ± 0.7 to 20.6 ± 0.7 wt% (samples PCPC1_01 and PCPC3_03 respectively, Table 3). On the contrary, the Na_2O contents are lower in the Cl-rich system (<11 wt%, see Table 3). In fact, carbonate melts become much richer in CaO (35.1 ± 5.6 and 36.8 ± 5.1 wt% of CaO, samples PCPC5_02 and PCPC5_03 in the

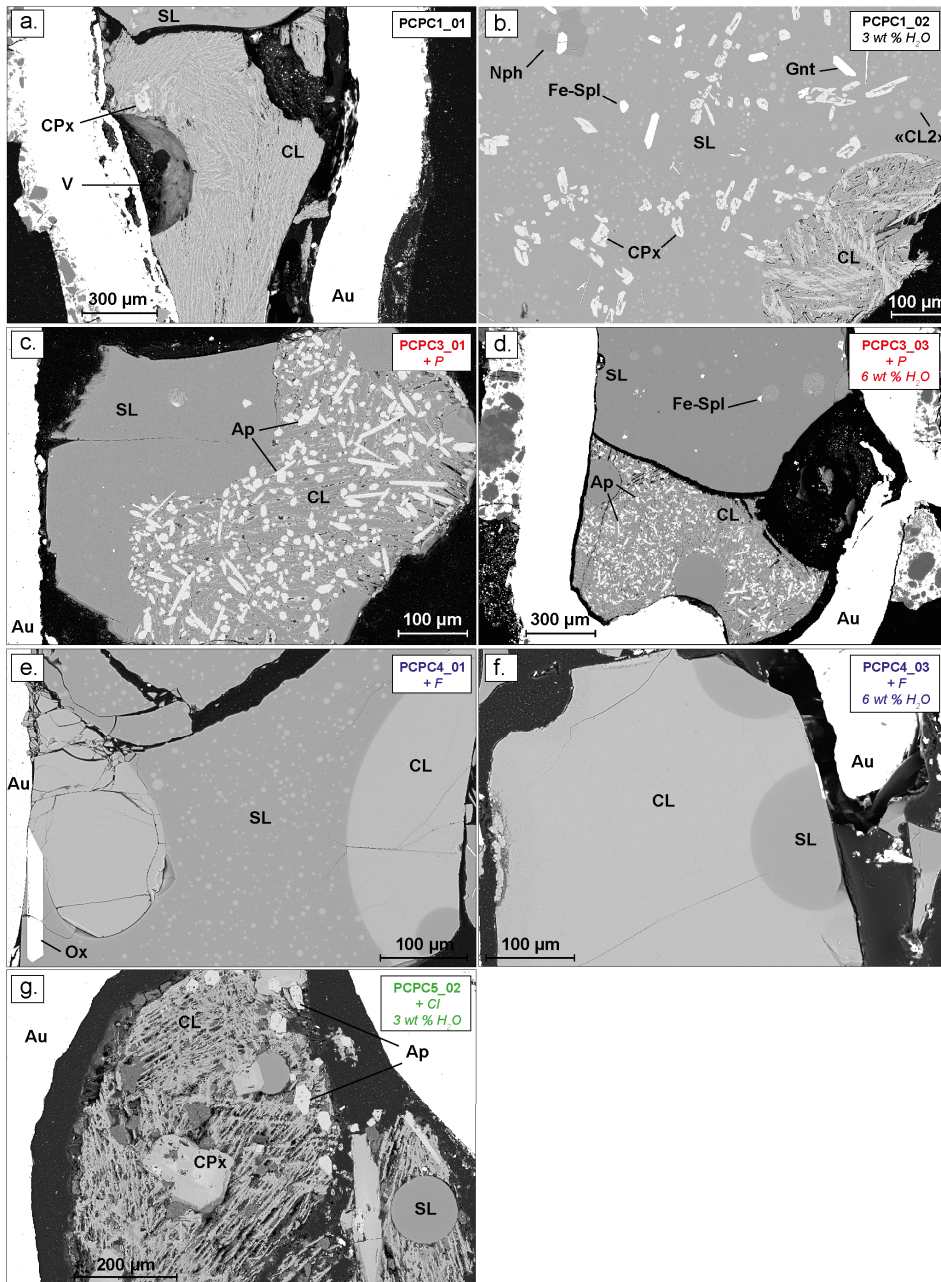


Figure 2. BSE images of typical experimental carbonate and silicate liquid immiscibility at 850 °C and 0.8 GPa, in the non-doped system in black (a and b), in the P-rich system in red (c and d); in the F-rich system in blue (e and f) and in the Cl-rich system in green (g). SL: silicate liquid; CL: carbonate liquid; CPx: clinopyroxene; Nph: nepheline; Gnt: garnet; Ap: apatite; Fe-Spl: ferrosplinel; Ox: Fe-Ti oxide; “CL2”: second carbonate liquid phase; V: fluid phase; Au: gold capsule.

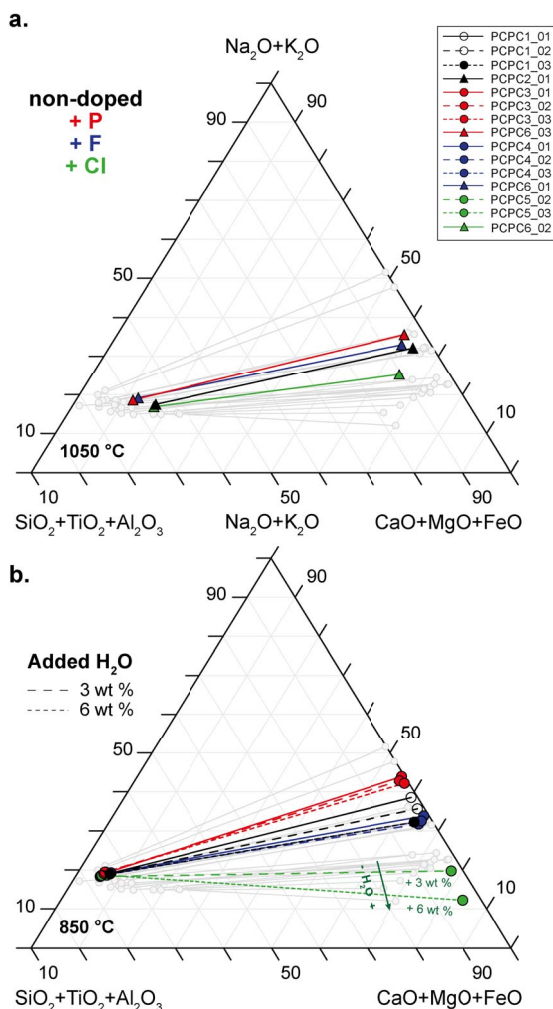


Figure 3. Hamilton projection of experimental immiscible silicate and carbonate liquids in the non-doped system and in P-, F- and Cl-rich systems at 0.8 GPa and 1050 °C (a) and 850 °C (b). Each line relates a pair of immiscible silicate and carbonate liquids in equilibrium at given P–T condition. Samples synthesized at both temperatures in the non-doped system (black), and in the systems doped in P (red), F (blue) and Cl (green) are represented, as well as hydrated samples (dashed line, 3 wt% of H₂O; dotted lines: 6 wt% of H₂O). The green arrow in (b) indicates the increase of sample H₂O contents in the Cl-rich systems (green). Carbonate and silicate melts of nephelinite–phonolite composition from Nabyl *et al.* [2020] are shown in grey. Empty symbols correspond to samples suspected to not be in equilibrium (PCPC1_01 and PCPC1_02).

Table 3) and poorer in Na₂O (8.2 ± 3.5 and 4.8 ± 2.3 wt% of Na₂O, Table 3) and K₂O (1.2 ± 0.7 and 0.8 ± 0.2 , Table 3) with increasing bulk water content (from 3 to 6 wt%; see the green arrow in Figure 3b). The carbonate melts thus slightly deviate from the (Na₂O

+ K₂O) pole and evolve towards the (CaO + MgO + FeO) pole (Figure 3b). This water effect that was predominant in the Cl-rich system is not observed in the non-doped system or the P- and F-rich systems (Figure 3b).

Table 3. Major element compositions of silicate and carbonate liquids (wt%) analysed by EMPA

	PCPC1_01		PCPC1_02		PCPC1_03		PCPC1_04		PCPC2_01		PCPC3_01		PCPC3_02	
<i>P</i> (Gpa)	0,8	<i>s.d.</i>	0,8	<i>s.d.</i>	0,8	<i>s.d.</i>	0,8	<i>s.d.</i>	0,8	<i>s.d.</i>	0,8	<i>s.d.</i>	0,8	<i>s.d.</i>
<i>T</i> (°C)	850		850		850		850		1050		850		850	
Starting material	<i>PhCbn1</i>		<i>PhCbn1</i>		<i>PhCbn1</i>		<i>PhCbn1</i>		<i>PhCbn1</i>		<i>PhCbn2</i>		<i>PhCbn2</i>	
Silicate liquid														
<i>N</i>	8	<i>s.d.</i>	7	<i>s.d.</i>	5	<i>s.d.</i>	11	<i>s.d.</i>	11	<i>s.d.</i>	8	<i>s.d.</i>	8	<i>s.d.</i>
SiO ₂	53.08	0.91	52.55	1.40	48.81	0.48	—	—	43.78	0.65	51.18	0.53	49.80	0.36
TiO ₂	0.38	0.10	<i>bdl</i>	—	0.40	0.08	—	—	0.52	0.09	0.44	0.08	0.51	0.05
Al ₂ O ₃	19.35	0.59	19.83	0.34	18.46	0.25	—	—	16.74	1.02	19.14	0.50	19.07	0.14
FeO	4.03	0.34	3.65	0.16	4.09	0.17	—	—	6.02	0.46	4.08	0.19	4.07	0.26
MnO	<i>bdl</i>	—	<i>bdl</i>	—	<i>bdl</i>	—	—	—	0.40	0.07	<i>bdl</i>	—	<i>bdl</i>	—
MgO	0.20	0.03	0.26	0.02	0.48	0.05	—	—	1.15	0.08	0.34	0.03	0.38	0.03
CaO	0.93	0.15	1.06	0.05	1.72	0.03	—	—	8.78	0.60	0.83	0.05	0.83	0.02
Na ₂ O	11.16	0.12	11.07	0.48	11.56	0.31	—	—	11.87	0.53	11.68	0.23	11.57	0.22
K ₂ O	6.60	0.20	6.47	0.39	5.69	0.27	—	—	4.38	0.29	6.15	0.16	6.39	0.15
P ₂ O ₅	<i>bdl</i>	—	<i>bdl</i>	—	<i>bdl</i>	—	—	—	0.30	0.06	0.20	0.03	<i>bdl</i>	—
BaO	<i>bdl</i>	—	0.15	0.01	0.20	0.01	—	—	0.37	0.03	0.14	0.01	0.15	0.02
SrO	<i>bdl</i>	—	<i>bdl</i>	—	<i>bdl</i>	—	—	—	0.44	0.05	<i>bdl</i>	—	<i>bdl</i>	—
SO ₂	<i>bdl</i>	—	<i>bdl</i>	—	<i>bdl</i>	—	—	—	<i>bdl</i>	—	<i>bdl</i>	—	<i>bdl</i>	—
F	0.41	0.09	0.39	0.07	0.32	0.06	—	—	0.55	0.11	0.41	0.07	0.37	0.08
Cl	0.07	0.01	0.07	0.01	0.07	0.01	—	—	0.06	0.01	0.08	0.01	0.08	0.01
Total	96.21	—	95.51	—	91.80	—	—	—	95.37	—	94.68	—	93.23	—
Na ₂ O + K ₂ O	17.76	0.32	17.54	0.87	17.26	0.58	—	—	16.25	0.82	17.83	0.38	17.96	0.37
ASI [Al ₂ O ₃ /(CaO + Na ₂ O + K ₂ O)]	0.71	—	0.73	—	0.65	—	—	—	0.42	—	0.70	—	0.69	—
NBO/T	0.25	—	0.24	—	0.32	—	—	—	0.75	—	0.27	—	0.28	—
(Na ₂ O + K ₂ O)/(CaO + MgO)	11.54	—	9.79	—	5.80	—	—	—	1.29	—	10.91	—	10.44	—
AI [Al ₂ O ₃ - (Na ₂ O + K ₂ O)]	-0.04	—	-0.04	—	-0.05	—	—	—	-0.05	—	-0.05	—	-0.05	—

(continued on next page)

Table 3. (continued)

	PCPC1_01	PCPC1_02	PCPC1_03	PCPC1_04	PCPC2_01	PCPC3_01	PCPC3_02
<i>P</i> (Gpa)	0.8	0.8	0.8	0.8	0.8	0.8	0.8
<i>T</i> (°C)	850	850	850	850	1050	850	850
Starting material	<i>PhCbn1</i>	<i>PhCbn1</i>	<i>PhCbn1</i>	<i>PhCbn1</i>	<i>PhCbn1</i>	<i>PhCbn2</i>	<i>PhCbn2</i>
Carbonate liquid							
<i>N</i>	6	8	8	8	9	6	6
	<i>s.d.</i>	<i>s.d.</i>	<i>s.d.</i>	<i>s.d.</i>	<i>s.d.</i>	<i>s.d.</i>	<i>s.d.</i>
SiO ₂	0.51	0.13	0.21	0.07	2.16	0.33	0.17
TiO ₂	<i>bdl</i>	—	<i>bdl</i>	—	<i>bdl</i>	—	—
Al ₂ O ₃	<i>bdl</i>	—	0.28	0.12	0.28	0.07	—
FeO	0.41	0.09	0.62	0.09	0.98	0.16	1.06
MnO	0.51	0.14	0.50	0.15	0.38	0.06	0.05
MgO	1.61	0.22	1.96	0.18	1.57	0.09	0.84
CaO	30.94	1.59	31.25	2.33	34.34	1.18	1.82
Na ₂ O	18.52	1.70	16.51	1.65	15.67	0.52	1.25
K ₂ O	2.55	0.21	2.33	0.22	2.89	0.22	0.16
P ₂ O ₅	1.92	0.24	1.82	0.16	2.75	0.26	0.06
BaO	1.16	0.14	1.24	0.07	0.99	0.07	0.85
SrO	1.66	0.15	1.69	0.20	1.56	0.14	0.30
SO ₂	0.28	0.05	0.33	0.12	0.13	0.03	0.10
F	2.91	0.13	2.95	0.32	2.07	0.22	1.34
Cl	0.15	0.04	0.12	0.02	0.31	0.01	0.26
Total	63.12	—	61.51	—	66.08	—	61.79
Na ₂ O + K ₂ O	21.07	1.91	18.84	1.86	18.56	0.75	1.41
					23.28	1.41	22.64
							1.00

(continued on next page)

Table 3. (continued)

P (Gpa)	PCPC3_03		PCPC3_04		PCPC4_01		PCPC4_02		PCPC4_03		PCPC4_04	
	0.8	850	0.8	850	0.8	850	0.8	850	0.8	850	0.8	850
Starting material	PhCbn2		PhCbn2		PhCbn3		PhCbn3		PhCbn3		PhCbn3	
Silicate liquid												
N	8	s.d.	8	s.d.	6	s.d.	11	s.d.	8	s.d.	8	s.d.
SiO ₂	50.15	0.57	—	—	53.67	0.81	47.83	0.68	50.36	0.26	—	—
TiO ₂	0.41	0.09	—	—	0.40	0.05	0.41	0.06	0.37	0.10	—	—
Al ₂ O ₃	19.33	0.35	—	—	19.10	0.46	18.03	0.34	19.16	0.37	—	—
FeO	4.08	0.35	—	—	4.32	0.31	4.36	0.21	4.04	0.27	—	—
MnO	bdl	—	—	—	bdl	—	bdl	—	0.28	0.04	—	—
MgO	0.33	0.03	—	—	0.26	0.05	0.34	0.02	0.26	0.02	—	—
CaO	0.81	0.04	—	—	0.81	0.08	1.56	0.06	1.12	0.05	—	—
Na ₂ O	11.88	0.13	—	—	10.99	0.10	11.63	0.11	11.42	0.21	—	—
K ₂ O	6.15	0.35	—	—	6.08	0.08	5.61	0.21	5.81	0.13	—	—
P ₂ O ₅	0.21	0.04	—	—	bdl	—	bdl	—	bdl	—	—	—
BaO	0.16	0.03	—	—	0.14	0.01	0.17	0.04	0.14	0.01	—	—
SrO	bdl	—	—	—	bdl	—	bdl	—	bdl	—	—	—
SO ₂	bdl	—	—	—	bdl	—	bdl	—	bdl	—	—	—
F	0.37	0.06	—	—	1.38	0.12	1.84	0.11	1.66	0.08	—	—
Cl	0.08	0.02	—	—	0.07	0.01	0.10	0.01	0.09	0.02	—	—
Total	93.96	—	—	—	97.21	—	91.88	—	94.71	—	—	—
Na ₂ O + K ₂ O	18.03	0.49	—	—	17.07	0.18	17.24	0.32	17.23	0.34	—	—
ASI [Al ₂ O ₃ /(CaO + Na ₂ O + K ₂ O)]	0.70	—	—	—	0.73	—	0.64	—	0.71	—	—	—
NBO/T	0.28	—	—	—	0.24	—	0.33	—	0.26	—	—	—
(Na ₂ O + K ₂ O)/(CaO + MgO)	11.45	—	—	—	11.65	—	6.82	—	9.36	—	—	—
AI [Al ₂ O ₃ - (Na ₂ O + K ₂ O)]	-0.05	—	—	—	-0.04	—	-0.05	—	-0.04	—	—	—

(continued on next page)

Table 3. (continued)

	PCPC3_03	PCPC3_04	PCPC4_01	PCPC4_02	PCPC4_03	PCPC4_04
<i>P</i> (Gpa)	0.8	0.8	0.8	0.8	0.8	0.8
<i>T</i> (°C)	850	850	850	850	850	850
Starting material	PhCbn2	PhCbn2	PhCbn3	PhCbn3	PhCbn3	PhCbn3
Carbonate liquid						
<i>N</i>	7	4	9	11	10	9
	s.d.	s.d.	s.d.	s.d.	s.d.	s.d.
SiO ₂	0.51	0.33	0.47	1.54	0.98	0.25
TiO ₂	bdl	0.29	bdl	bdl	bdl	bdl
Al ₂ O ₃	bdl	—	0.15	0.31	0.28	bdl
FeO	2.57	3.34	0.36	0.40	0.40	2.79
MnO	0.70	0.70	0.58	0.52	0.48	0.44
MgO	2.89	2.18	2.88	2.39	2.53	2.14
CaO	25.43	25.44	34.27	34.65	33.92	30.59
Na ₂ O	20.62	20.95	17.46	16.03	16.22	20.49
K ₂ O	2.22	3.45	1.95	2.17	2.10	2.44
P ₂ O ₅	2.99	2.76	1.81	1.96	1.92	1.83
BaO	1.54	1.46	1.13	1.01	0.98	0.50
SrO	1.65	1.75	1.93	1.85	2.19	1.21
SO ₂	0.31	0.31	0.25	0.30	0.38	0.17
F	2.54	3.57	10.92	11.46	10.70	11.35
Cl	0.37	0.74	0.53	0.46	0.55	0.35
Total	64.34	67.26	74.67	75.03	73.63	74.54
Na ₂ O + K ₂ O	22.83	24.40	19.42	18.20	18.32	22.93
	1.49	1.23	0.40	0.45	1.27	0.95

(continued on next page)

Table 3. (continued)

Starting material	PCPC5_02		PCPC5_03		PCPC5_04		PCPC6_01		PCPC6_02		PCPC6_03	
	0.8	850	0.8	850	0.8	850	0.8	1050	0.8	1050	0.8	850
	PhCbn5	PhCbn6	PhCbn7	PhCbn3	PhCbn4	PhCbn2						
Silicate liquid												
<i>N</i>	7	s.d.	18	s.d.	17	s.d.	3	s.d.	6	s.d.		
SiO ₂	50.07	0.45	45.79	0.86	—	—	42.92	0.47	46.32	0.22	46.32	0.60
TiO ₂	0.30	—	bdl	—	—	—	0.42	0.10	0.48	0.03	0.48	0.10
Al ₂ O ₃	20.54	0.32	19.54	0.28	—	—	16.34	0.28	18.50	0.34	18.50	0.25
FeO	2.40	0.25	2.48	0.19	—	—	5.34	0.34	5.69	0.24	5.69	0.19
MnO	bdl	—	bdl	—	—	—	bdl	0.05	bdl	—	bdl	—
MgO	0.34	0.02	0.45	0.04	—	—	1.02	0.04	0.77	0.03	0.77	0.03
CaO	2.08	0.05	2.64	0.04	—	—	9.00	0.30	4.64	0.19	4.64	0.17
Na ₂ O	11.65	0.20	11.18	0.41	—	—	11.40	0.39	12.78	0.23	12.78	0.26
K ₂ O	5.28	0.14	5.02	0.19	—	—	3.75	0.19	4.62	0.06	4.62	0.23
P ₂ O ₅	bdl	—	bdl	—	—	—	0.37	0.05	0.95	0.05	0.95	0.11
BaO	0.17	0.02	0.25	0.04	—	—	0.34	0.05	0.29	0.05	0.29	0.05
SrO	bdl	—	bdl	—	—	—	0.52	0.06	bdl	0.04	bdl	—
SO ₂	bdl	—	bdl	—	—	—	bdl	—	bdl	—	bdl	—
F	0.43	0.07	1.00	0.07	—	—	0.73	0.83	0.56	0.03	0.56	0.07
Cl	0.77	0.01	0.83	0.02	—	—	1.29	0.01	0.11	0.02	0.11	0.02
Total	94.03	—	89.18	—	—	—	93.44	—	95.69	—	95.69	—
Na ₂ O + K ₂ O	16.94	0.34	16.21	0.59	—	—	15.15	0.58	17.40	0.28	17.40	0.49
ASI [Al ₂ O ₃ /(CaO + Na ₂ O + K ₂ O)]	0.72	—	0.68	—	—	—	0.42	—	0.54	—	0.54	—
NBO/T	0.23	—	0.28	—	—	—	0.73	—	0.52	—	0.52	—
(Na ₂ O + K ₂ O)/(CaO + MgO)	5.37	—	4.01	—	—	—	1.20	—	2.51	—	2.51	—
AI [Al ₂ O ₃ - (Na ₂ O + K ₂ O)]	-0.03	—	-0.03	—	—	—	-0.04	—	-0.05	—	-0.05	—

(continued on next page)

Table 3. (continued)

	PCPC5_02	PCPC5_03	PCPC5_04	PCPC6_01	PCPC6_02	PCPC6_03
<i>P</i> (Gpa)	0.8	0.8	0.8	0.8	0.8	0.8
<i>T</i> (°C)	850	850	850	1050	1050	850
Starting material	PhCbn5	PhCbn6	PhCbn7	PhCbn3	PhCbn4	PhCbn2
Carbonate liquid						
<i>N</i>	7	s.d.	11	s.d.	6	7
SiO ₂	1.02	0.36	1.49	0.68	0.04	2.87
TiO ₂	—	—	bdl	—	0.18	0.01
Al ₂ O ₃	bdl	—	0.30	0.19	bdl	0.60
FeO	0.32	0.07	0.43	0.17	1.89	1.25
MnO	0.51	0.13	0.58	0.16	0.42	0.41
MgO	1.70	0.30	1.86	0.48	0.89	2.10
CaO	35.10	5.62	36.82	5.11	29.35	33.10
Na ₂ O	8.18	3.53	4.84	2.34	15.94	16.66
K ₂ O	1.19	0.67	0.82	0.21	3.95	3.01
P ₂ O ₅	1.53	0.40	1.48	0.44	1.49	1.75
BaO	1.53	0.25	1.60	0.12	0.82	1.04
SrO	2.22	0.22	2.17	0.27	1.43	1.59
SO ₂	0.25	0.08	0.38	0.25	0.27	0.25
F	3.52	0.80	5.63	0.75	—	11.79
Cl	0.73	0.25	0.59	0.30	3.23	0.51
Total	57.80	—	59.00	—	77.10	—
Na ₂ O + K ₂ O	9.37	4.20	5.66	2.55	19.89	1.78
						19.67
						0.52
						13.02
						1.75
						19.63
						0.80

N: number of analysis; bdl: below detection limit; s.d.: standard deviation; ASI: alumina saturation index; Al: alkaline index; NBO/T: non-bridging oxygen per tetrahedrally coordinated cation. The ASI, NBO/T, alkali/alkaline-earth ratio and NBO/T are in molar fractions; Italics: samples in which equilibrium between carbonate and silicate liquids is assumed not to have been attained.

A second carbonate liquid phase is observed in two samples from the non-doped system that were synthesized at 850 °C (PCPC1_01 and PCPC1_02, Table 2; see Figure 3b, empty black circles). In comparison to the main carbonate melts (Table 3), this second carbonate liquid is rare, presents higher CaO concentrations and higher totals during the EMPA analyses (see Supplementary Table 1). The occurrence of this second carbonate phase suggests that the equilibrium was not achieved in these two samples. When plotted in the chemical diagrams (see results and discussion sections, empty black circles in figures), the corresponding data points are outliers. For the sake of clarity, these two samples are included in the diagrams, but are not discussed further here.

The F, Cl and P₂O₅ silicate melt concentrations at 850 °C for all the systems are lower than those at 1050 °C. In the non-doped system (see Table 2), the silicate melts contain relatively small amounts of F (0.3–0.4 wt%), Cl (0.07 wt%), and P₂O₅ is below the detection limit (samples PCPC1, Table 3). The concentrations are slightly higher in F, Cl or P doped systems (Table 2), varying from 1.4 to 1.8 wt% for F in the F-rich system (samples PCPC4, Table 3), 0.6 to 0.8 wt% for the Cl in the Cl-rich system (samples PCPC5, Table 3) and only around 0.2 wt% for the P₂O₅ in the P-rich system (samples PCPC3, Table 3). Carbonate melts are also more enriched in those elements at the higher temperature, although P₂O₅ and Cl carbonate melt concentrations remain low in the P- and Cl-doped systems respectively (see samples PCPC3 and PCPC5_05, Table 3).

Trace element concentrations—including the REE—of both silicate and carbonate melts are presented in Table 4. At 1050 °C, the silicate melts contain 18.2 ± 0.5 to 35.9 ± 0.7 ppm of La as representative of other LREE (light REE), and 32.1 ± 0.9 to 50.3 ± 0.7 ppm of Lu, as representative of other HREE (high REE; Table 4), whereas REE concentrations in the carbonate melts are higher and vary from 87.6 ± 2.8 to 108.1 ± 5.6 for La and 50.0 ± 2.3 to 74.9 ± 2.7 ppm for Lu (Table 4). The silicate melt REE concentrations are lower at 850 °C, varying from 1.8 ± 0.0 to 8.4 ± 0.1 ppm of La, and from 3.9 ± 0.0 to 17.87 ± 3.1 ppm of Lu (Table 4). At this temperature, carbonate melt REE concentrations are generally much higher than at 1050 °C, varying from 77.7 ± 5.4 to 140.5 ± 9.8 ppm and 51.6 ± 3.3 to 116.2 ± 5.2 for La and Lu re-

spectively (Table 4). In the Cl-rich system, the middle REE and high REE (MREE and HREE) concentrations decrease slightly in the carbonate melts with increasing water content (67.0 ± 1.9 to 34.8 ± 5.0 ppm of Gd and 34.0 ± 1.3 to 13.0 ± 1.9 ppm of Lu, samples PCPC5_02 to PCPC5_03, from 3 to 6 wt% of water; Table 4), whereas no significant variation in concentration is observed in the silicate melts (Table 4). This behaviour is not observed in other chemical systems.

3.3. REE partitioning between carbonate and silicate liquids

Trace element partitioning is defined using the Nernst partition coefficient D which corresponds to the mass concentration ratio in ppm of the element x in the carbonate liquid (CL) and the silicate liquid (SL; $D_x^{CL/SL} = x^{CL}/x^{SL}$). Trace element partition coefficients (including REE) are presented in the Table 5.

Figure 4 presents REE partition coefficients for the four chemical systems investigated. For all samples and for all experimental conditions, REE partition coefficients vary greatly, by almost two orders of magnitude. The large $D_{REE}^{CL/SL}$ variation observed in the literature [Hamilton *et al.*, 1989, Martin *et al.*, 2013, Nabyl *et al.*, 2020, Veksler *et al.*, 2012, 1998] also occurs in F-, Cl- and P-rich systems. The $D_{REE}^{CL/SL}$ are higher for LREE (light REE) than for HREE (heavy REE). For most charges in the four chemical systems, carbonate melts are richer in REE than silicate melts ($D_{REE}^{CL/SL} > 1$, Figure 4). At 850 °C, the $D_{REE}^{CL/SL}$ in the non-doped system vary from 10.7 ± 2.2 to 29.6 ± 3.3 for La and from 1.7 ± 0.3 to 5.8 ± 1.1 for Lu (Figure 4). The carbonate melt REE enrichment is greater in the P- and F-rich systems (Figure 4), being almost two times higher than in the non-doped system, with the $D_{La}^{CL/SL}$ varying from 37.1 ± 4.1 to 46.2 ± 6.2 and from 26.5 ± 1.8 to 43.0 ± 5.7 in the P- and the F-rich systems respectively, and the $D_{Lu}^{CL/SL}$ varying from 5.6 ± 0.4 to 6.8 ± 0.5 and from 7.3 ± 1.8 to 8.7 ± 2.0 (Figure 4, Table 5).

No clear effect of water on REE partitioning is identified in the non-doped system and the P- and F-rich systems (Figure 4 and Table 5). In the Cl-rich system, the REE partition coefficients decrease with the addition of water (3 and 6 wt% of water, samples PCPC5_02 and PCPC5_03, Table 2), from 21.3 ± 1.6 to 14.8 ± 2.0 for $D_{La}^{CL/SL}$ and 4.6 ± 0.5 to 3.3 ± 0.5

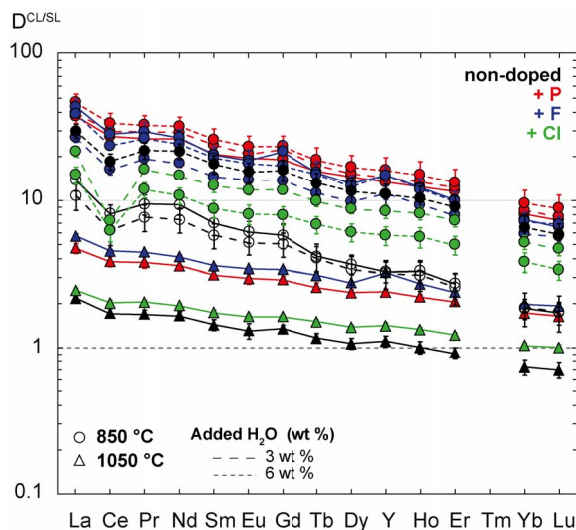


Figure 4. REE partition coefficients ($D^{\text{CL/SL}}$) between carbonate and silicate liquids (CL and SL), in the non-doped system in black, the P-rich system in red, the F-rich system in blue and the Cl-rich system in green. Samples synthesized at 850 °C (circles) and at 1050 °C (triangles) are shown in all chemical systems, as well as hydrated samples (dashed line, 3 wt% of H_2O ; dotted lines: 6 wt% of H_2O). Empty symbols correspond to samples suspected to not be in equilibrium (PCPC1_01 and PCPC1_02).

for $D_{\text{Lu}}^{\text{CL/SL}}$ (samples PCPC5_02 and PCPC5_03, green dashed and dotted lines in Figure 4).

For some samples, the Ce partition coefficients show a negative anomaly. The $D_{\text{Ce}}^{\text{CL/SL}}$ is lower compared to that of other LREE. This is particularly marked in Cl-rich samples (PCPC5_02 and PCPC5_03, green circles in Figure 4; Table 5), in the non-doped system (samples PCPC1_01 to PCPC1_03, black circles in Figure 4; Table 5) and in the F-rich system (PCPC4_02, blue circles in Figure 4; Table 5). This $D_{\text{Ce}}^{\text{CL/SL}}$ decrease reflects the higher Ce concentrations in the silicate liquids for all these samples compared to other LREE, whereas the carbonate melt Ce concentrations do not present any particular variation (see Tables 4 and 5).

At the higher temperature (1050 °C, triangles in Figure 4), the carbonate melt enrichments in REE are lower in all four chemical systems, especially in the non-doped system with a $D_{\text{La}}^{\text{CL/SL}}$ and a $D_{\text{Lu}}^{\text{CL/SL}}$ of 2.2 ± 0.1 and 0.7 ± 0.1 respectively (Table 5). As for the experiments at 850 °C, REE partitioning is more in favour of carbonate liquids for samples doped in P and F (red and blue triangles, Figure 4), with a $D_{\text{La}}^{\text{CL/SL}}$ of 4.7 ± 0.4 and 5.7 ± 0.2 respectively in the P- and

F-rich systems, and a $D_{\text{Lu}}^{\text{CL/SL}}$ of 1.6 ± 0.1 and 1.9 ± 0.1 (Table 5).

To summarise the REE partitioning, the experimental $D_{\text{REE}}^{\text{CL/SL}}$ vary by two orders of magnitude; their values increase as temperature decreases and in addition are higher in the F- and P-rich systems. Nabyl *et al.* [2020] proposed an equation relating the REE partitioning between carbonate and silicate melts to the degree of alkaline silicate melt differentiation (i.e. composition, alkalinity and polymerisation of the silicate melt). The question arises as to whether this silicate melt composition effect still applies in systems rich in F, Cl or P, or whether these elements play a key role in REE concentrations in F-, Cl- or P-rich systems. This is tested below.

4. Discussion

4.1. REE partitioning: silicate melt composition effect in F-, Cl- and P-rich environments?

In order to investigate the effect of F, Cl and P on $D_{\text{REE}}^{\text{CL/SL}}$, we compared the data in this study with the model presented in Nabyl *et al.* [2020]. The latter, which does not consider F, Cl and P, uses parameters

Table 4. Trace element concentrations of silicate and carbonate liquids (ppm) measured by LA-ICP-MS

	PCPCI_01*		PCPCI_02*		PCPCI_03*		PCPCI_04*		PCPC2_01*		PCPC3_01*	
<i>P</i> (Gpa)	0.8	0.8	0.8	0.8	0.8	0.8	0.8	0.8	0.8	0.8	0.8	0.8
<i>T</i> (°C)	850	850	850	850	850	850	850	1050	1050	850	850	850
Starting material	<i>PhCbn1</i>	<i>PhCbn1</i>	<i>PhCbn1</i>	<i>PhCbn1</i>	<i>PhCbn1</i>	<i>PhCbn1</i>	<i>PhCbn1</i>	<i>PhCbn1</i>	<i>PhCbn1</i>	<i>PhCbn1</i>	<i>PhCbn1</i>	<i>PhCbn2</i>
Silicate liquid												
<i>N</i>	7	<i>s.d.</i>	7	<i>s.d.</i>	6	<i>s.d.</i>	6	<i>s.d.</i>	9	<i>s.d.</i>	7	<i>s.d.</i>
<i>Sc</i>	15.17	3.54	34.96	9.76	21.84	2.90	—	—	82.89	4.24	39.25	1.95
<i>Ti</i>	1722.11	126.26	2282.59	426.48	862.60	52.74	—	—	2239.38	98.18	1867.08	114.38
<i>Cr</i>	<i>bdl</i>	—	6.07	1.61	1.66	0.32	—	—	105.21	5.28	3.56	1.88
<i>Mn</i>	903.56	56.98	1249.54	445.68	472.90	29.53	—	—	2159.03	70.74	537.31	17.23
<i>Sr</i>	450.72	16.06	730.14	95.67	397.74	2.44	—	—	2572.65	43.23	378.68	4.86
<i>Zr</i>	580.26	43.20	755.17	128.74	279.51	16.76	—	—	523.19	31.47	464.28	12.99
<i>Nb</i>	208.32	14.51	295.54	58.84	86.68	5.53	—	—	176.48	6.98	180.16	10.04
<i>Ba</i>	777.66	22.57	1171.89	201.80	622.28	8.40	—	—	2544.81	100.89	709.05	15.87
<i>La</i>	6.68	1.08	10.92	2.21	2.97	0.31	—	—	33.60	1.38	2.10	0.10
<i>Ce</i>	11.66	1.69	19.87	4.01	4.90	0.60	—	—	41.67	2.20	2.85	0.15
<i>Pr</i>	8.18	1.28	13.96	2.75	3.54	0.44	—	—	34.81	1.66	2.37	0.15
<i>Nd</i>	8.50	1.30	14.35	2.69	3.60	0.44	—	—	36.38	1.61	2.38	0.15
<i>Sm</i>	10.90	1.90	18.12	3.35	4.10	0.56	—	—	42.00	2.30	2.87	0.16
<i>Eu</i>	13.11	2.09	22.11	3.77	4.85	0.70	—	—	52.00	4.21	3.57	0.23
<i>Gd</i>	13.41	2.50	19.50	3.55	4.44	0.71	—	—	36.74	1.61	2.99	0.09
<i>Tb</i>	16.47	3.23	23.05	4.18	5.47	0.87	—	—	39.11	1.82	3.92	0.35
<i>Dy</i>	19.24	2.62	30.66	5.85	6.04	1.08	—	—	47.94	2.80	5.26	0.49
<i>Y</i>	23.46	3.38	35.93	7.17	6.88	1.16	—	—	52.38	2.92	6.78	0.64
<i>Ho</i>	21.41	3.29	33.41	6.63	6.65	1.27	—	—	51.99	3.21	6.16	0.61
<i>Er</i>	22.16	3.61	35.07	6.85	6.59	1.27	—	—	47.54	2.70	6.78	0.71
<i>Yb</i>	32.06	3.89	48.50	9.54	9.11	1.72	—	—	58.23	4.26	10.90	1.08
<i>Lu</i>	29.42	4.06	45.02	9.25	8.90	1.61	—	—	52.45	4.03	11.02	1.12

(continued on next page)

Table 4. (continued)

	PCPCI_01*	PCPCI_02*	PCPCI_03*	PCPCI_04*	PCPC2_01*	PCPC3_01*						
<i>P</i> (Gpa)	0.8	0.8	0.8	—	0.8	0.8						
<i>T</i> (°C)	850	850	850	—	1050	850						
Starting material	PhCbn1	PhCbn1	PhCbn1	—	PhCbn1	PhCbn2						
Hf	42.35	18.44	42.85	14.25	15.37	1.18	—	23.17	2.78	15.84	1.02	
Ta	15.29	1.89	15.59	4.41	5.16	0.72	—	13.42	1.17	8.95	2.80	
Carbonate liquid												
<i>N</i>	7	<i>s.d.</i>	8	<i>s.d.</i>	8	<i>s.d.</i>	8	<i>s.d.</i>	9	<i>s.d.</i>	6	<i>s.d.</i>
Sc	16.55	5.58	25.72	8.22	36.68	3.68	5.91	0.22	22.82	1.82	67.67	9.06
Ti	417.75	71.91	435.16	69.26	635.91	66.01	409.73	19.12	512.03	37.31	524.79	162.22
Cr	—	0.60	4.82	0.85	9.57	1.03	3.46	0.34	36.49	1.65	4.00	2.08
Mn	2856.29	336.42	3187.73	618.01	3047.76	286.54	1976.40	64.70	2164.52	82.90	4819.84	598.04
Sr	10765.74	186.60	11208.43	521.58	10494.11	272.33	10980.47	308.52	10543.97	151.78	9573.38	166.70
Zr	12.66	3.19	13.89	2.12	29.88	4.17	29.38	1.71	22.59	5.48	17.15	12.49
Nb	123.19	8.08	115.54	9.70	119.03	10.82	145.17	8.26	96.08	5.11	87.58	24.27
Ba	8306.41	374.70	8108.73	627.56	8532.66	584.38	6905.15	377.24	7382.78	327.68	8069.63	581.14
La	91.07	1.98	116.82	6.49	87.67	3.65	90.47	4.53	72.46	2.86	78.08	7.79
Ce	93.48	2.08	122.93	8.30	89.68	3.12	96.01	4.06	70.92	3.68	77.12	7.43
Pr	76.58	2.16	106.25	5.08	76.86	2.96	74.04	2.62	58.55	2.79	62.00	6.58
Nd	78.65	2.30	105.17	5.24	77.34	2.47	75.45	2.26	59.56	2.77	62.59	5.46
Sm	75.31	2.60	104.14	5.49	71.88	2.43	75.98	2.65	59.58	4.04	58.47	10.20
Eu	79.58	3.70	113.03	5.70	75.24	2.78	76.19	1.88	67.33	6.10	68.66	11.71
Gd	76.86	3.68	97.65	3.41	70.44	2.80	69.95	1.78	49.04	2.51	56.22	10.39
Tb	67.96	4.73	92.25	7.70	71.14	3.45	61.83	1.41	45.09	2.29	61.10	11.06
Dy	70.10	4.78	103.01	10.52	68.82	2.97	63.68	1.63	50.73	3.25	75.93	16.02
Y	76.37	4.96	113.69	10.32	74.80	4.51	72.33	2.32	57.64	3.96	88.99	18.30
Ho	70.32	5.51	102.89	10.96	68.12	3.74	62.39	1.70	51.94	3.89	75.80	14.71
Er	59.78	4.72	89.49	11.25	59.12	3.44	53.15	1.53	43.34	3.14	77.41	13.70

(continued on next page)

Table 4. (continued)

	PCPC1_01*	PCPC1_02*	PCPC1_03*	PCPC1_04*	PCPC2_01*	PCPC3_01*						
<i>P</i> (Gpa)	0.8	0.8	0.8	0.8	0.8	0.8						
<i>T</i> (°C)	850	850	850	850	1050	850						
Starting material	PhCbn1	PhCbn1	PhCbn1	PhCbn1	PhCbn1	PhCbn2						
Yb	59.02	5.90	90.03	14.80	58.81	3.93	46.64	1.18	42.16	3.92	86.84	19.02
Lu	50.68	5.59	78.83	13.92	51.55	3.33	37.47	1.06	36.27	3.45	80.26	17.71
Hf	0.52	0.20	0.48	0.09	1.08	0.14	0.61	0.06	0.64	0.11	0.48	0.39
Ta	1.29	0.13	1.08	0.26	1.73	0.23	2.57	0.42	2.77	0.44	0.68	0.29
	PCPC3_02*	PCPC3_03*	PCPC4_01*	PCPC4_02*	PCPC4_03*	PCPC4_04*						
<i>P</i> (Gpa)	0.8	0.8	0.8	0.8	0.8	0.8						
<i>T</i> (°C)	850	850	850	850	850	850						
Starting material	PhCbn2	PhCbn2	PhCbn3	PhCbn3	PhCbn3	PhCbn3						
Silicate liquid												
<i>N</i>	7	s.d.	6	s.d.	10	s.d.	7	s.d.	7	s.d.	7	s.d.
Sc	39.91	1.22	34.95	0.65	50.18	5.94	41.81	1.33	35.83	1.34	—	—
Ti	1760.76	70.24	1757.33	62.49	1748.28	167.15	1833.56	25.31	1797.32	24.89	—	—
Cr	3.40	0.51	2.24	0.51	5.87	4.27	2.91	0.21	2.66	0.60	—	—
Mn	558.63	15.79	513.90	7.26	808.71	98.81	957.86	21.90	770.69	14.67	—	—
Sr	374.99	4.69	362.90	2.65	402.67	23.67	659.56	22.10	514.72	17.37	—	—
Zr	453.15	13.88	452.70	21.67	540.17	42.31	486.15	11.39	483.61	5.61	—	—
Nb	167.10	6.54	208.97	3.42	162.48	111.38	185.76	36.18	119.17	7.10	—	—
Ba	714.74	14.37	681.30	4.34	591.25	42.20	867.69	25.01	638.31	9.81	—	—
La	1.98	0.02	1.80	0.05	2.99	0.38	4.16	0.11	2.84	0.10	—	—
Ce	2.69	0.05	2.41	0.09	5.12	0.56	7.38	0.21	4.89	0.29	—	—
Pr	2.16	0.02	1.97	0.07	4.43	0.63	5.22	0.18	3.73	0.19	—	—
Nd	2.18	0.03	1.99	0.05	4.86	0.60	5.76	0.16	3.99	0.22	—	—
Sm	2.61	0.08	2.43	0.06	6.50	0.84	7.42	0.28	5.10	0.35	—	—
Eu	3.13	0.08	3.01	0.14	7.51	1.34	6.97	0.15	5.43	0.28	—	—
Gd	2.96	0.09	2.79	0.14	7.36	0.99	8.64	0.54	5.88	0.47	—	—

(continued on next page)

Table 4. (continued)

P (Gpa)	PCPC3_02*		PCPC3_03*		PCPC4_01*		PCPC4_02*		PCPC4_03*		PCPC4_04*	
	0.8	850	0.8	850	0.8	850	0.8	850	0.8	850	0.8	850
Starting material	PhCbn2	PhCbn2	PhCbn2	PhCbn2	PhCbn3	PhCbn3	PhCbn3	PhCbn3	PhCbn3	PhCbn3	PhCbn3	PhCbn3
Tb	3.43	0.11	3.33	0.19	8.65	1.36	8.16	0.44	5.58	0.39	—	—
Dy	4.86	0.18	4.46	0.22	11.54	1.53	10.55	0.35	7.89	0.50	—	—
Y	6.12	0.24	5.63	0.34	11.18	1.50	10.71	0.37	7.83	0.42	—	—
Ho	5.63	0.25	5.17	0.35	12.28	1.77	10.79	0.48	8.35	0.55	—	—
Er	6.32	0.27	5.68	0.42	13.57	1.79	11.61	0.51	9.01	0.59	—	—
Yb	10.16	0.52	9.25	0.76	19.66	2.54	16.43	0.66	13.11	0.92	—	—
Lu	10.11	0.48	9.15	0.69	17.87	3.07	13.94	0.54	11.07	0.71	—	—
Hf	20.77	3.60	18.89	0.66	14.49	1.50	27.54	4.84	28.19	1.77	—	—
Ta	10.89	2.03	11.80	0.62	4.89	3.69	22.92	6.98	9.06	4.48	—	—
Carbonate liquid												
N	6	s.d.	7	s.d.	5	s.d.	11	s.d.	6	s.d.	5	s.d.
Sc	73.11	11.04	79.57	10.03	88.83	3.83	75.85	3.24	72.39	2.74	82.41	2.03
Ti	520.20	164.35	947.61	137.79	475.87	30.90	729.92	60.19	674.37	16.28	1002.95	40.94
Cr	8.65	2.55	5.82	0.06	2.44	0.69	7.12	1.29	5.99	1.37	5.83	1.13
Mn	5113.86	470.08	4822.68	496.32	4107.32	273.08	3301.18	196.25	3389.16	80.25	3615.10	25.16
Sr	9528.76	617.79	10292.20	513.75	13647.83	164.16	12793.00	533.91	13799.87	463.88	9027.72	125.16
Zr	7.69	1.33	28.71	8.40	9.08	1.73	26.99	7.01	18.93	3.35	173.69	33.16
Nb	92.84	22.37	180.84	31.09	44.97	4.73	153.34	23.82	84.49	8.25	228.43	9.65
Ba	7819.33	1186.38	9474.97	646.82	8228.87	120.45	7843.84	342.81	7263.80	123.90	4263.01	81.33
La	77.67	5.41	83.11	10.93	128.67	4.97	110.32	7.00	109.17	3.15	103.41	2.06
Ce	78.80	4.66	80.27	13.66	143.52	5.61	118.43	8.38	114.60	3.09	111.10	2.37
Pr	62.89	4.31	63.51	10.11	129.00	6.05	99.80	5.61	97.82	2.30	91.90	1.30
Nd	62.80	2.42	63.22	9.21	129.24	4.66	102.55	5.95	95.36	3.17	94.32	1.63
Sm	61.74	2.41	62.71	11.02	131.42	5.42	106.40	7.04	98.00	5.48	91.60	1.68

(continued on next page)

Table 4. (continued)

	PCPC3_02*		PCPC3_03*		PCPC4_01*		PCPC4_02*		PCPC4_03*		PCPC4_04*	
<i>P</i> (Gpa)	0.8	0.8	0.8	0.8	0.8	0.8	0.8	0.8	0.8	0.8	0.8	0.8
<i>T</i> (°C)	850	850	850	850	850	850	850	850	850	850	850	850
Starting material	PhCbn2	PhCbn2	PhCbn2	PhCbn2	PhCbn3	PhCbn3	PhCbn3	PhCbn3	PhCbn3	PhCbn3	PhCbn3	PhCbn3
Eu	64.14	3.02	69.32	12.07	139.11	7.44	95.41	4.07	95.56	2.75	106.80	1.87
Gd	65.22	8.07	64.83	10.61	156.76	16.55	116.71	11.75	100.35	5.81	105.18	1.88
Tb	58.92	3.79	62.08	13.19	132.83	11.91	90.71	5.50	82.88	3.88	84.93	1.79
Dy	73.55	4.50	74.34	15.22	148.93	6.75	102.40	5.93	97.33	4.23	96.41	2.05
Y	86.94	6.30	89.67	18.97	164.07	8.28	117.38	8.64	115.00	4.72	106.62	3.30
Ho	74.60	4.72	76.56	17.44	148.44	7.26	99.67	6.93	98.73	3.94	93.68	1.71
Er	76.80	5.96	74.88	15.38	134.91	5.56	91.03	4.64	88.10	3.78	86.27	1.54
Yb	85.98	7.47	87.28	19.17	143.49	5.25	96.00	6.00	92.84	3.86	92.06	1.71
Lu	77.40	6.02	79.99	17.27	116.18	5.21	78.27	4.53	75.25	2.97	74.34	1.52
Hf	0.27	0.07	0.70	0.26	0.21	0.04	0.90	0.23	0.76	0.24	4.56	1.00
Ta	0.55	0.25	1.72	0.34	0.29	0.34	3.44	1.12	1.35	0.56	1.69	0.16
	PCPC5_02**#		PCPC5_03*		PCPC5_04*		PCPC6_01*		PCPC6_02*		PCPC6_03#	
<i>P</i> (Gpa)	0.8	0.8	0.8	0.8	0.8	0.8	0.8	0.8	0.8	0.8	0.8	0.8
<i>T</i> (°C)	850	850	850	850	1050	1050	1050	1050	1050	1050	1050	1050
Starting material	PhCbn4	PhCbn4	PhCbn4	PhCbn4	PhCbn3	PhCbn3	PhCbn3	PhCbn3	PhCbn3	PhCbn3	PhCbn2	PhCbn2
Silicate liquid												
<i>N</i>	3	s.d.	6	s.d.	6	s.d.	6	s.d.	6	s.d.	6	s.d.
Sc	6.05	0.20	5.77	0.14	—	—	66.59	3.94	74.22	1.07	88.83	1.42
Ti	612.58	13.30	527.99	5.43	—	—	2402.61	154.04	2361.75	35.60	2868.19	71.36
Cr	bdl	—	1.83	0.26	—	—	98.02	4.99	66.76	1.03	107.96	7.94
Mn	639.17	38.43	910.95	7.22	—	—	1770.07	66.64	1863.55	24.96	2023.31	26.64
Sr	974.34	19.03	1211.86	14.66	—	—	1825.38	37.09	3296.04	48.13	2484.08	19.47
Zr	310.69	8.11	284.47	3.79	—	—	517.10	33.40	468.16	7.35	662.16	26.19
Nb	116.31	1.80	115.81	1.13	—	—	233.27	10.97	239.08	1.87	207.30	6.47

(continued on next page)

Table 4. (continued)

	PCPC5_02*#	PCPC5_03*	PCPC5_04*	PCPC6_01*	PCPC6_02*	PCPC6_03#						
<i>P</i> (Gpa)	0.8	0.8	—	0.8	0.8	0.8						
<i>T</i> (°C)	850	850	—	1050	1050	1050						
Starting material	PhCbn4	PhCbn4	—	PhCbn3	PhCbn3	PhCbn2						
Ba	1095.46	8.07	1696.68	25.25	—	2033.84	61.31	2442.04	42.44	2623.17	31.88	
La	6.60	0.14	8.37	0.11	—	18.21	0.48	35.92	0.66	23.13	1.32	
Ce	15.09	0.31	15.99	0.21	—	23.70	0.37	46.62	0.77	28.81	1.44	
Pr	6.33	0.02	7.77	0.08	—	20.08	0.35	36.54	0.72	23.44	1.30	
Nd	6.41	0.03	7.08	0.08	—	20.94	0.42	37.34	0.55	23.94	1.14	
Sm	5.98	0.26	6.32	0.18	—	22.86	0.37	40.86	0.87	28.88	0.98	
Eu	5.80	0.19	5.10	0.05	—	25.18	0.40	42.14	0.93	31.18	1.32	
Gd	5.01	0.05	4.42	0.09	—	31.75	0.74	45.63	0.95	31.76	1.77	
Tb	3.99	0.12	4.01	0.04	—	25.62	0.36	43.41	0.67	29.91	1.28	
Dy	4.74	0.06	4.01	0.05	—	29.94	0.61	46.50	0.89	37.06	1.02	
Y	5.49	0.18	5.02	0.07	—	31.02	0.71	51.43	0.76	42.40	1.36	
Ho	4.37	0.22	3.80	0.03	—	31.57	0.71	49.84	0.76	39.05	1.39	
Er	4.07	0.22	3.49	0.03	—	29.83	0.75	43.62	0.66	39.36	1.25	
Yb	5.16	0.12	4.21	0.05	—	36.48	0.94	52.56	1.12	50.36	0.94	
Lu	4.79	0.16	3.90	0.05	—	32.12	0.87	50.31	0.68	45.94	1.04	
Hf	12.26	0.65	10.04	0.12	—	36.48	1.49	15.90	0.27	31.21	1.12	
Ta	7.64	0.25	8.86	0.18	—	1.73	0.09	14.07	0.23	6.37	1.10	
Carbonate liquid												
<i>N</i>	7	s.d.	8	s.d.	8	s.d.	7	s.d.	11	s.d.	6	s.d.
<i>Sc</i>	6.54	1.00	4.86	1.03	9.98	0.42	53.15	0.62	36.92	1.98	64.64	7.37
<i>Ti</i>	328.34	63.91	265.10	52.93	448.59	26.27	841.60	21.28	1033.07	100.60	1193.03	124.36
<i>Cr</i>	—	2.80	14.53	3.77	7.88	0.54	69.66	2.12	94.58	12.42	100.91	15.54

(continued on next page)

Table 4. (continued)

P (Gpa)	PCPC5_02**		PCPC5_03*		PCPC5_04*		PCPC6_01*		PCPC6_02*		PCPC6_03#	
	0.8	850	0.8	850	0.8	850	0.8	1050	0.8	1050	0.8	1050
T (°C)	PhCbn4		PhCbn4		PhCbn3		PhCbn3		PhCbn3		PhCbn2	
Mn	3690.77	532.50	4723.97	458.62	2943.49	77.26	2743.15	10.07	2853.87	140.87	4062.84	308.27
Sr	16991.89	1297.96	15848.10	915.96	10373.42	135.30	11368.69	66.30	11250.34	278.61	13607.86	562.29
Zr	10.28	2.59	8.24	2.64	29.31	1.62	46.92	2.45	51.76	7.86	57.89	6.78
Nb	132.66	28.73	129.93	28.67	188.87	6.85	175.58	2.36	201.28	17.62	180.34	10.51
Ba	10845.25	1728.56	11756.56	1482.52	6453.81	136.46	7706.21	52.41	6960.76	441.99	10612.55	1058.95
La	140.48	9.79	123.54	16.44	86.77	1.75	103.32	1.14	87.61	2.83	108.09	5.60
Ce	109.18	5.91	98.47	15.28	87.22	1.52	106.09	1.30	93.18	3.99	109.41	6.24
Pr	102.18	5.17	90.71	10.68	68.96	0.89	88.55	0.92	74.01	1.74	87.87	6.57
Nd	93.26	4.04	75.43	9.52	68.67	1.16	85.81	1.25	71.65	1.60	85.18	5.29
Sm	74.46	7.05	54.76	7.35	63.84	0.94	81.48	0.96	70.41	2.21	89.29	4.43
Eu	67.40	4.29	40.70	5.99	66.39	0.85	85.87	1.03	68.30	1.83	91.13	6.05
Gd	58.29	3.35	34.76	5.02	61.28	0.77	106.95	1.29	73.71	1.66	90.98	2.21
Tb	38.98	2.92	27.20	3.59	52.04	0.66	78.63	1.08	64.90	2.08	76.11	4.48
Dy	40.86	2.84	24.11	3.43	61.00	0.61	81.70	0.86	63.89	1.67	86.96	2.73
Y	45.83	4.36	28.71	4.21	70.66	1.35	99.27	0.63	72.43	2.56	101.05	2.86
Ho	35.37	2.84	21.24	3.39	59.44	0.72	84.56	1.24	66.00	2.24	85.78	1.70
Er	29.38	2.47	17.15	2.54	52.29	0.82	70.44	0.80	52.85	1.48	80.40	1.70
Yb	26.53	2.94	15.95	2.41	50.14	0.91	71.53	0.95	54.14	1.95	86.00	1.71
Lu	22.24	2.27	13.01	1.93	37.57	0.95	61.22	0.90	50.05	2.31	74.90	2.73
Hf	0.20	0.09	0.26	0.06	4.48	0.20	2.19	0.11	1.37	0.22	1.58	0.24
Ta	1.50	0.25	1.82	0.48	0.71	0.03	0.49	0.01	4.56	0.54	1.85	0.33

N: number of analysis; Bdl: below detection limit; s.d.: standard deviation. Italics: samples in which equilibrium between carbonate and silicate liquids is assumed not to have been attained. *: sample analysed by the Agilent 7500 CS Quadrupole ICP-MS; #: sample analysed by the Agilent 7900 Quadrupole ICP-MS.

Table 5. Partition coefficients between silicate and carbonate liquids, for Ca, volatiles and trace elements

P (Gpa)	PCPC1_01		PCPC1_02		PCPC1_03		PCPC2_01		PCPC3_01		PCPC3_02		PCPC3_03		PCPC4_01	
	0,8	850	0,8	850	0,8	850	0,8	1050	0,8	850	0,8	850	0,8	850	0,8	850
T (°C)	PhCbn1 s.d.		PhCbn1 s.d.		PhCbn1 s.d.		PhCbn1 s.d.		PhCbn2 s.d.		PhCbn2 s.d.		PhCbn2 s.d.		PhCbn3 s.d.	
Ca	33.10	5.69	29.47	2.65	18.00	0.89	3.91	0.89	0.30	29.43	2.87	29.99	1.84	31.55	3.85	42.46
F	7.140	1.549	7.469	1.587	7.200	1.591	3.786	0.855	7.322	3.496	6.378	1.762	6.806	2.060	7.913	0.731
Cl	2.160	0.620	1.866	0.405	0.626	0.194	5.126	0.492	5.039	3.316	2.497	1.290	4.442	1.880	7.725	1.576
P ₂ O ₅	—	—	—	—	—	—	9.018	1.961	8.601	1.339	—	—	14.365	4.824	—	—
Sc	1.091	0.447	0.736	0.312	1.679	0.279	0.275	0.026	1.724	0.246	1.832	0.282	2.277	0.290	1.770	0.223
Ti	0.243	0.045	0.191	0.047	0.737	0.089	0.229	0.019	0.281	0.089	0.295	0.094	0.539	0.081	0.272	0.031
Cr	—	—	0.794	0.253	5.765	1.275	0.347	0.023	1.125	0.834	2.541	0.839	2.602	0.591	0.416	0.324
Mn	3.161	0.422	2.551	1.036	6.445	0.727	1.003	0.051	8.970	1.150	9.154	0.880	9.384	0.975	5.079	0.706
Sr	23.886	0.946	15.351	2.135	26.384	0.704	4.098	0.091	25.281	0.547	25.411	1.678	28.361	1.431	33.893	2.034
Zr	0.022	0.006	0.018	0.004	0.107	0.016	0.043	0.011	0.037	0.027	0.017	0.003	0.063	0.019	0.017	0.003
Nb	0.591	0.057	0.391	0.084	1.373	0.153	0.544	0.036	0.486	0.137	0.556	0.136	0.865	0.149	0.277	0.192
Ba	10.681	0.573	6.919	1.306	13.712	0.957	2.901	0.173	11.381	0.858	10.940	1.674	13.907	0.954	13.918	1.014
La	13.628	2.220	10.695	2.245	29.565	3.317	2.157	0.123	37.141	4.098	39.217	2.758	46.195	6.208	43.034	5.710
Ce	8.018	1.177	6.187	1.316	18.315	2.333	1.702	0.126	27.094	2.979	29.346	1.819	33.307	5.803	28.026	3.260
Pr	9.361	1.489	7.613	1.546	21.738	2.822	1.682	0.113	26.168	3.236	29.077	2.013	32.250	5.257	29.153	4.360
Nd	9.254	1.445	7.329	1.422	21.513	2.695	1.637	0.105	26.306	2.833	28.744	1.196	31.753	4.703	26.577	3.440
Sm	6.908	1.229	5.746	1.104	17.553	2.470	1.419	0.124	20.382	3.731	23.672	1.192	25.788	4.574	20.209	2.744
Eu	6.070	1.010	5.113	0.909	15.512	2.317	1.295	0.157	19.210	3.509	20.506	1.107	23.052	4.146	18.531	3.453
Gd	5.731	1.103	5.008	0.927	15.882	2.606	1.335	0.090	18.818	3.520	22.038	2.800	23.198	3.966	21.308	3.644
Tb	4.126	0.859	4.002	0.798	13.002	2.172	1.153	0.079	15.582	3.150	17.171	1.227	18.660	4.103	15.360	2.780

(continued on next page)

Table 5. (continued)

	PCPCI_01	PCPCI_02	PCPCI_03	PCPC2_01	PCPC3_01	PCPC3_02	PCPC3_03	PCPC4_01								
<i>P</i> (Gpa)	0,8	0,8	0,8	0,8	0,8	0,8	0,8	0,8								
<i>T</i> (°C)	850	850	850	1050	850	850	850	850								
Starting material	<i>PhCbn1</i> s.d.	<i>PhCbn1</i> s.d.	<i>PhCbn1</i> s.d.	<i>PhCbn1</i> s.d.	<i>PhCbn2</i> s.d.	<i>PhCbn2</i> s.d.	<i>PhCbn2</i> s.d.	<i>PhCbn3</i> s.d.								
Dy	3.644	0.554	3.359	0.727	11.400	2.099	1.058	0.092	14.427	3.328	15.148	1.080	16.656	3.508	12.903	1.803
Y	3.255	0.515	3.164	0.694	10.880	1.956	1.100	0.097	13.125	2.966	14.208	1.173	15.918	3.504	14.671	2.109
Ho	3.285	0.567	3.080	0.694	10.251	2.039	0.999	0.097	12.297	2.678	13.240	1.025	14.809	3.517	12.092	1.844
Er	2.698	0.488	2.552	0.593	8.966	1.798	0.912	0.084	11.413	2.347	12.161	1.080	13.194	2.877	9.939	1.373
Yb	1.841	0.290	1.856	0.476	6.456	1.291	0.724	0.086	7.969	1.916	8.459	0.851	9.439	2.214	7.298	0.980
Lu	1.723	0.305	1.751	0.475	5.790	1.112	0.692	0.084	7.281	1.769	7.657	0.698	8.739	1.999	6.501	1.155
Hf	0.012	0.007	0.011	0.004	0.070	0.010	0.027	0.006	0.030	0.025	0.013	0.004	0.037	0.014	0.015	0.003
Ta	0.084	0.013	0.069	0.026	0.336	0.064	0.206	0.037	0.076	0.040	0.050	0.025	0.146	0.030	0.059	0.082
	PCPC4_02	PCPC4_03	PCPC5_02	PCPC5_03	PCPC6_01	PCPC6_02	PCPC6_03									
<i>P</i> (Gpa)	0.8	0.8	0.8	0.8	0.8	0.8	0.8									
<i>T</i> (°C)	850	850	850	850	1050	1050	1050									
Starting material	<i>PhCbn3</i> s.d.	<i>PhCbn3</i> s.d.	<i>PhCbn4</i> s.d.	<i>PhCbn4</i> s.d.	<i>PhCbn3</i> s.d.	<i>PhCbn4</i> s.d.	<i>PhCbn2</i> s.d.									
Ca	22.24	0.86	30.40	1.56	16.89	2.74	13.93	1.95	6.64	0.42	3.32	0.23	6.34	0.31		
F	6.225	0.408	6.442	0.333	8.245	2.285	5.630	0.834	3.060	0.684	4.933	1.058	4.204	0.706		
Cl	4.680	0.493	6.288	1.281	0.950	0.329	0.718	0.368	5.883	0.992	0.706	0.257	4.423	1.481		
P ₂ O ₅	—	—	—	—	—	—	—	—	11.747	3.925	5.418	2.925	9.934	1.542		
Sc	1.814	0.097	2.020	0.108	1.082	0.169	0.843	0.179	0.798	0.048	0.497	0.028	0.728	0.084		
Ti	0.398	0.033	0.375	0.010	0.536	0.105	0.502	0.100	0.350	0.024	0.437	0.043	0.416	0.045		
Cr	2.448	0.477	2.254	0.727	—	—	7.956	2.357	0.711	0.042	1.417	0.187	0.935	0.159		
Mn	3.446	0.220	4.398	0.134	5.774	0.903	5.186	0.505	1.550	0.059	1.531	0.078	2.008	0.155		

(continued on next page)

Table 5. (continued)

Starting material	PCPC4_02		PCPC4_03		PCPC5_02		PCPC5_03		PCPC6_01		PCPC6_02		PCPC6_03	
	P (Gpa)	T (°C)	0.8	850	0.8	850	0.8	850	0.8	1050	0.8	1050	0.8	1050
	PhCbn3	s.d.	PhCbn3	s.d.	PhCbn4	s.d.	PhCbn4	s.d.	PhCbn3	s.d.	PhCbn4	s.d.	PhCbn2	s.d.
Sr	19.396	1.038	26.811	1.277	17.439	1.375	13.077	0.772	6.228	0.132	3.413	0.098	5.478	0.230
Zr	0.056	0.014	0.039	0.007	0.033	0.008	0.029	0.009	0.091	0.008	0.111	0.017	0.087	0.011
Nb	0.825	0.206	0.709	0.081	1.141	0.248	1.122	0.248	0.753	0.037	0.842	0.074	0.870	0.057
Ba	9.040	0.473	11.380	0.261	9.900	1.580	6.929	0.880	3.789	0.117	2.850	0.188	4.046	0.407
La	26.519	1.831	38.475	1.709	21.285	1.549	14.759	1.973	5.675	0.161	2.439	0.091	4.672	0.360
Ce	16.054	1.222	23.416	1.509	7.234	0.419	6.159	0.959	4.477	0.089	1.999	0.092	3.797	0.288
Pr	19.135	1.254	26.194	1.478	16.133	0.818	11.682	1.380	4.411	0.089	2.025	0.062	3.749	0.349
Nd	17.799	1.145	23.924	1.551	14.557	0.634	10.659	1.351	4.099	0.102	1.919	0.051	3.558	0.279
Sm	14.348	1.093	19.231	1.704	12.459	1.296	8.671	1.189	3.565	0.071	1.723	0.065	3.092	0.186
Eu	13.685	0.657	17.603	1.035	11.621	0.832	7.980	1.178	3.410	0.068	1.621	0.056	2.922	0.230
Gd	13.513	1.602	17.062	1.686	11.634	0.678	7.869	1.147	3.369	0.089	1.616	0.050	2.864	0.174
Tb	11.120	0.901	14.841	1.238	9.761	0.789	6.782	0.897	3.069	0.060	1.495	0.053	2.544	0.185
Dy	9.706	0.647	12.329	0.947	8.621	0.610	6.010	0.859	2.729	0.062	1.374	0.044	2.347	0.098
Y	10.960	0.889	14.687	0.987	8.353	0.838	5.715	0.843	3.200	0.076	1.408	0.054	2.383	0.102
Ho	9.234	0.763	11.817	0.907	8.093	0.764	5.597	0.893	2.678	0.072	1.324	0.049	2.197	0.090
Er	7.843	0.527	9.781	0.768	7.225	0.725	4.915	0.729	2.361	0.065	1.212	0.039	2.043	0.078
Yb	5.844	0.435	7.084	0.577	5.145	0.581	3.787	0.574	1.961	0.057	1.030	0.043	1.708	0.047
Lu	5.615	0.390	6.797	0.513	4.639	0.497	3.338	0.496	1.906	0.059	0.995	0.048	1.631	0.070
Hf	0.033	0.010	0.027	0.009	0.016	0.007	0.026	0.006	0.060	0.004	0.086	0.014	0.051	0.008
Ta	0.150	0.067	0.149	0.096	0.197	0.034	0.206	0.055	0.281	0.017	0.324	0.038	0.291	0.072

s.d.: standard deviation, calculated statistical uncertainty. Italics: samples in which equilibrium between carbonate and silicate liquids is assumed not to have been attained.

related to the silicate melt composition and structure to define $D_{La}^{CL/SL}$ (La being used as representative of other REE) for all samples from the four chemical systems. These parameters are:

- the CaO content, which is a good proxy of mineral fractionation during alkaline magma differentiation (Figure 5a, Table 3);
- the alumina saturation index, abbreviated to ASI ($Al_2O_3/(CaO + Na_2O + K_2O)$; Figure 5b, Table 3), which indicates the degree of peralkalinity of the silicate melt; we note here that all the silicate liquids from this study are peralkaline, with an ASI < 1 and a negative alkalinity index (abbreviated to A.I. in Table 3);
- the alkali/alkaline-earth cation ratio ($(Na_2O + K_2O)/(CaO + MgO)$, Figure 5c).

In this discussion, we also systematically use the NBO/T [non-bridging oxygen per tetrahedrally coordinated cation; Mysen *et al.*, 1982], a classic parameter used to indicate the degree of polymerisation of silicate melts (Figure 5d).

For the 19 samples synthesized at 850–1050 °C and 0.8 GPa, in the four chemical systems (non-doped, + F, + Cl or + P) and \pm additional water (Table 2), the $D_{La}^{CL/SL}$ decreases while the silicate melt CaO contents increase (Figure 5a). This effect indicates that REE-rich carbonate melts (high $D_{La}^{CL/SL}$) coexist with fractionated silicate liquids (i.e. with low CaO contents) in all chemical systems, including those doped in F, Cl and P. The $D_{La}^{CL/SL}$ also correlates with the ASI of the silicate melts (Figure 5b): the most peralkaline silicate liquid (ASI < 0.5 in Figure 5b; samples PCPC2_01, PCPC6_01 and PCPC6_02, Table 3) corresponds to the lowest $D_{La}^{CL/SL}$ (Table 5), whereas less peralkaline silicate liquids (ASI > 0.6, Figure 5b) have the highest $D_{La}^{CL/SL}$. Moreover, $D_{La}^{CL/SL}$ increases with the $(Na_2O + K_2O)/(CaO + MgO)$ ratio (Figure 5c): as this ratio increases (representing an increase in alkali in the silicate melts relative to the CaO and the MgO contents; Figure 5c and Table 3), the REE concentrations in the conjugate carbonate melts increase; this is observed in all charges whether or not doped in F, Cl and P. Lastly, Figure 5d shows an inverse correlation between $D_{La}^{CL/SL}$ and NBO/T, with $D_{La}^{CL/SL}$ increasing as NBO/T decreases (indicating a more polymerised silicate liquid). These effects have also all been observed in previous investigations on immiscible carbonate and

alkaline silicate melts [grey symbols in Figure 5; Hamilton *et al.*, 1989, Martin *et al.*, 2013, Nabyl *et al.*, 2020, Veksler *et al.*, 2012, 1998]. In both non-doped and F-, Cl- and P-doped systems, REE-rich carbonate melts can coexist with highly fractionated (low CaO, Figure 5a), weakly peralkaline (low ASI and AI, Figure 5b and Table 3) and highly polymerised (low NBO/T, Figure 5d) alkaline silicate melts. The trends shown in Figure 5 do not allow any sub-systems to be distinguished.

4.2. *The role of F, Cl and P in the silicate melt composition*

As suggested by Figure 5, the highest REE partition coefficients, which correspond to the F- and P-rich charges (Figures 4 and 5), demonstrate that the conjugate silicate melts are among the most fractionated, the least peralkaline and the most polymerised silicate melts. This could suggest that the addition of F and P has an impact on the composition of the silicate melts in equilibrium with carbonate melts. As described in the Introduction section, the addition of F, Cl and P has important effects on the physical properties of silicate melts. However, the new data in this study show that, only F or Cl could have a significant effect on the silicate melt structure and composition, since P_2O_5 concentrations are generally below the detection limit for all the experimental charges (see Table 3).

It has been shown that the addition of water, the composition of the silicate melt and the F concentration all affect F speciation in synthetic peralkaline silicate melts [Baasner *et al.*, 2014]. Baasner *et al.* [2013a] also highlighted that the effect of Cl on the silicate melt structure depends on the melt composition, and that Cl and F have opposing effects on peralkaline silicate melt viscosity: Cl increases the viscosity, whereas F decreases it. Thus the F and Cl effects could impact the structure and composition of the peralkaline silicate melts of nephelinite-phonolite type used in this study, and consequently the REE partitioning between carbonate and silicate melts.

The F and Cl partition coefficients (see Table 5) are plotted in Figure 6 against NBO/T and ASI which are taken as proxies of the silicate melt composition and structure. $D_F^{CL/SL}$ values are in the range of 5–9 (Table 5) and show weak negative and positive

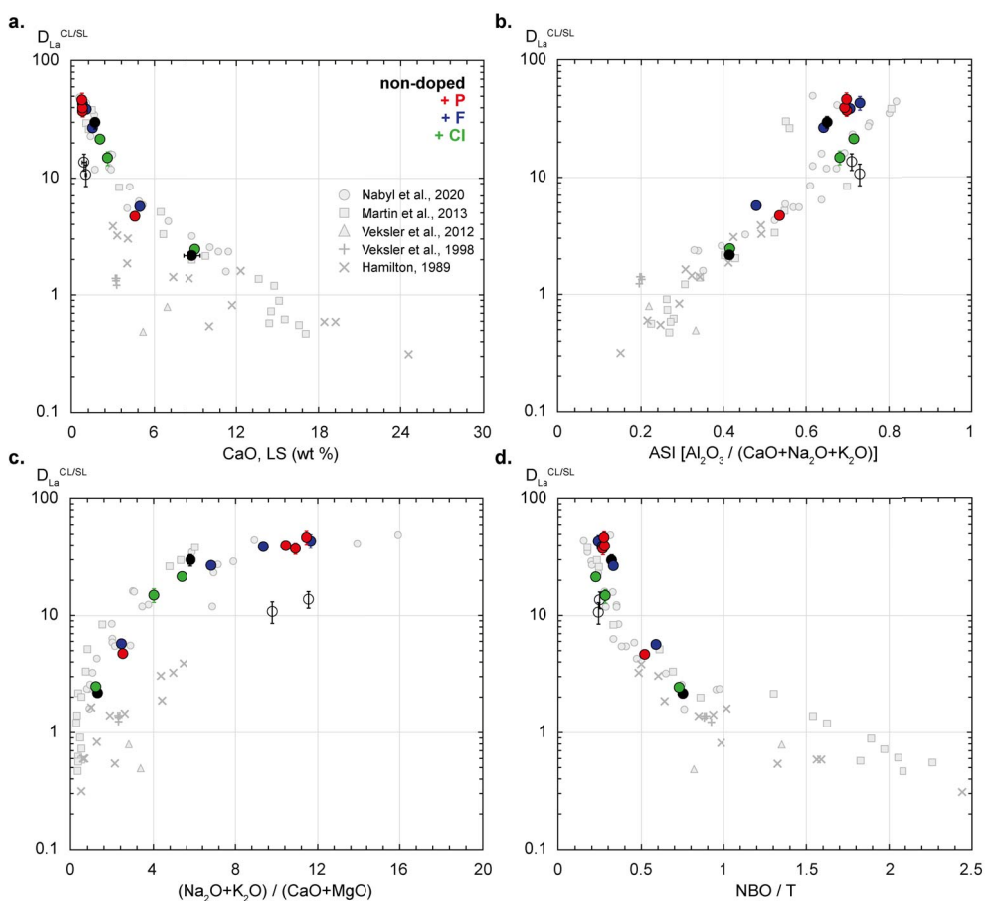


Figure 5. Silicate melt composition and structure effects on the La partition coefficient ($D_{La}^{CL/SL}$) between carbonate and silicate liquids (CL and SL), for all the samples synthesized in the four chemical systems (in black for the system with no additional volatile, red for the P-rich system, blue for the F-rich system and green for the Cl-rich system), at 850 °C–1050 °C–0.8 GPa and \pm additional H₂O. The $D_{La}^{CL/SL}$ are represented against the CaO concentrations in wt% (a), the ASI (alumina saturation index; b), the alkali/alkaline-earth cation ratio (c) and the NBO/T (d) of the silicate liquids. The grey symbols correspond to previous experimental studies on carbonate and silicate melt immiscibility [Hamilton *et al.*, 1989, Martin *et al.*, 2013, Nabyl *et al.*, 2020, Veksler *et al.*, 2012, 1998]. Empty symbols correspond to samples suspected to not be in equilibrium (PCPC1_01 and PCPC1_02).

correlations with NBO/T (Figure 6a) and ASI parameters (Figure 6b) respectively. $D_{Cl}^{CL/SL}$ values range from 0.6 to 8, but show no correlation with either the composition or the structure of the silicate melt (Figures 6c–d). We note, however, that $D_{Cl}^{CL/SL}$ values are much lower for Cl-rich systems.

No clear correlation between $D_{REE}^{CL/SL}$ and the silicate–carbonate melt F and Cl contents has emerged so far (see Supplementary Figure 1), nei-

ther in this study nor in previous investigations (grey symbols, Supplementary Figure 1). REE seem to concentrate in carbonate melts (high $D_{REE}^{CL/SL}$), which can coexist with both F-/Cl-rich silicate melts and F-/Cl-poor silicate melts. Furthermore, no relationship has been observed between La and either F or Cl partitioning (Table 5). This suggests that no significant direct effect of volatile concentrations on carbonate–silicate melt REE partitioning has been detected.

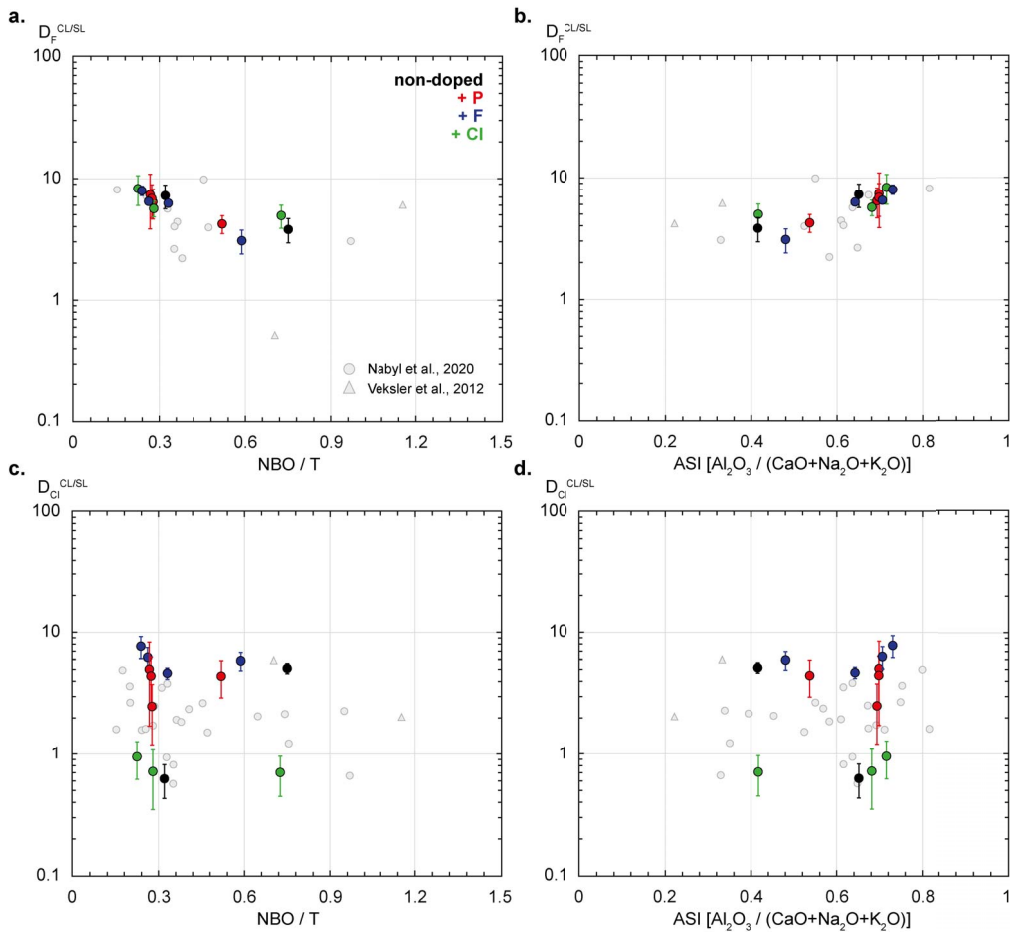


Figure 6. Fluorine and chlorine partition coefficients between carbonate and silicate liquids (CL and SL; $D_F^{CL/SL}$ and $D_{Cl}^{CL/SL}$ respectively) plotted against the silicate melt NBO/T (a and b, molar fraction) and the ASI (c and d; molar fraction). All samples synthesized in the four chemical systems (in black for the system with no additional volatile, red for the P-rich system, blue for the F-rich system and green for the Cl-rich system), at 850 °C–1050 °C–0.8 GPa and \pm additional H₂O are shown. The grey symbols correspond to previous experimental studies on carbonate and silicate melt immiscibility [Nabyl et al., 2020, Veksler et al., 2012].

The lower $D_{Ce}^{CL/SL}$ compared with other LREE (see Section 3.3; Figure 4) appear to be related to slightly higher Ce concentrations in the silicate melts (Table 4). This may be linked to Ce–F complexes which form in the silicate melt structure, as suggested by Ponader and Brown [1989] for La, Gd and Yb. Alternatively, the negative $D_{Ce}^{CL/SL}$ anomaly could reflect a change in oxidation state of Ce in the silicate melt. This element usually occurs in the Ce³⁺ form, but can also occur in the less common oxidised

form Ce⁴⁺ [Adachi and Imanaka, 1998, Burnham and Berry, 2014]. Burnham and Berry [2014] have shown that Ce³⁺ remains the dominant form in the silicate melts, but also that the stability of Ce⁴⁺ can be enhanced in depolymerised silicate melts in synthetic systems (SMFAC–Ce system). The negative $D_{Ce}^{CL/SL}$ anomaly could therefore be explained by the oxidation of Ce³⁺ to Ce⁴⁺. This anomaly is low at 850 °C in the non-doped system and in the F-rich systems (black and blue lines respectively, Figure 4),

but is particularly marked in the Cl-rich systems (green lines, Figure 4). This suggests that Cl-rich samples are more oxidised and that the oxidation state could favour the formation of Ce^{4+} -Cl complexes. However, it is not possible at this stage to reach any definite conclusions on the redox state and its impact on the behaviour of Ce.

4.3. Prediction of carbonate melt REE contents in F-Cl-P-rich systems

4.3.1. Application of the carbonatite REE enrichment model to F-, Cl- and P-rich systems

The REE partitioning model between carbonate and silicate liquids of Nabyl et al. [2020] relates $D_{\text{Ca}}^{\text{CL/SL}}$ and $D_{\text{REE}}^{\text{CL/SL}}$ to the silicate melt composition. This model is based on the correlation between $D_{\text{Ca}}^{\text{CL/SL}}$ and $D_{\text{REE}}^{\text{CL/SL}}$ shown in Figure 7 for La, including both data from the literature [Hamilton et al., 1989, Martin et al., 2013, Nabyl et al., 2020, Veksler et al., 2012] and the new data in this work. The data points illustrating the systems doped in F, Cl and P are indistinguishable from the literature data containing much lower amounts of these elements (Figure 7).

The Nabyl et al. [2020] partitioning equations have been used to calculate $D_{\text{Ca}}^{\text{CL/SL}}$ and $D_{\text{REE}}^{\text{CL/SL}}$ for the F-, Cl- and P-rich samples. In detail, the calculations are carried out as follows (see the online application tools, <http://calcul-isto.cnrs-orleans.fr/apps/REE-carb-melt/>):

The $D_{\text{Ca}}^{\text{CL/SL}}$ were calculated using three parameters relating to the silicate melt composition (the SiO_2 content in wt%, the ASI and the $(\text{Na}_2\text{O} + \text{K}_2\text{O})/(\text{CaO} + \text{MgO})$ ratio in molar fraction) in the following equation:

$$\ln(D_{\text{Ca}}^{\text{CL/SL}}) = a_0 + a_1 * \text{SiO}_2 + a_2 * \frac{\text{Al}_2\text{O}_3}{(\text{CaO} + \text{Na}_2\text{O} + \text{K}_2\text{O})} + a_3 * \frac{(\text{Na}_2\text{O} + \text{K}_2\text{O})}{(\text{CaO} + \text{MgO})}. \quad (1)$$

The $D_{\text{REE}}^{\text{CL/SL}}$ were estimated from the calculated $D_{\text{Ca}}^{\text{CL/SL}}$ based on the correlation shown in Figure 7 for La, and for all the other REE [Nabyl et al., 2020]:

$$D_{\text{REE}}^{\text{CL/SL}} = a * (D_{\text{Ca}}^{\text{CL/SL}})^b. \quad (2)$$

The calculated $D_{\text{Ca}}^{\text{CL/SL}}$ and $D_{\text{La}}^{\text{CL/SL}}$ from this model are plotted against the measured $D_{\text{Ca}}^{\text{CL/SL}}$ and $D_{\text{La}}^{\text{CL/SL}}$ (Figures 8a and b respectively). Both the $D_{\text{Ca}}^{\text{CL/SL}}$ and $D_{\text{La}}^{\text{CL/SL}}$ values for the F-, Cl- and P-rich systems are

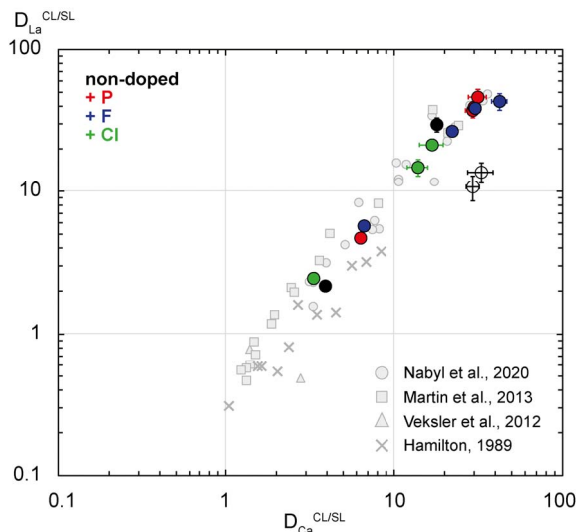


Figure 7. La partition coefficients ($D_{\text{La}}^{\text{CL/SL}}$) versus Ca partition coefficient ($D_{\text{Ca}}^{\text{CL/SL}}$) between carbonate and silicate liquids (CL and SL), for all the samples synthesized in the four chemical systems (in black for the system with no additional volatile, red for the P-rich system, blue for the F-rich system and green for the Cl-rich system), at 850 °C–1050 °C–0.8 GPa and \pm additional H_2O . Previous experimental studies of carbonate and silicate melt immiscibility are also represented [grey symbols; Hamilton et al., 1989, Veksler et al., 2012, Martin et al., 2013, Nabyl et al., 2020]. Empty symbols correspond to samples suspected to not be in equilibrium (PCPC1_01 and PCPC1_02).

well reproduced (close to the 1-1 line; Figure 8) and fall in the compositional field of the experimental studies used to calibrate the model (grey field, Figure 8). The REE partitioning model of Nabyl et al. [2020] predicts, within uncertainty, the measured REE partition coefficients in the F, Cl and P enriched magmatic systems.

Although the two partitioning data points from the secondary carbonate liquid phase (“CL2”, see Section 3.2; Figure 1b) are outliers in Figures 7 and 8b (empty black circles), they are also well-predicted in terms of $D_{\text{Ca}}^{\text{CL/SL}}$ (Figure 8a). This suggests that the Ca partitioning between the carbonate and silicate liquids is in equilibrium, unlike the case of trace elements including REE.

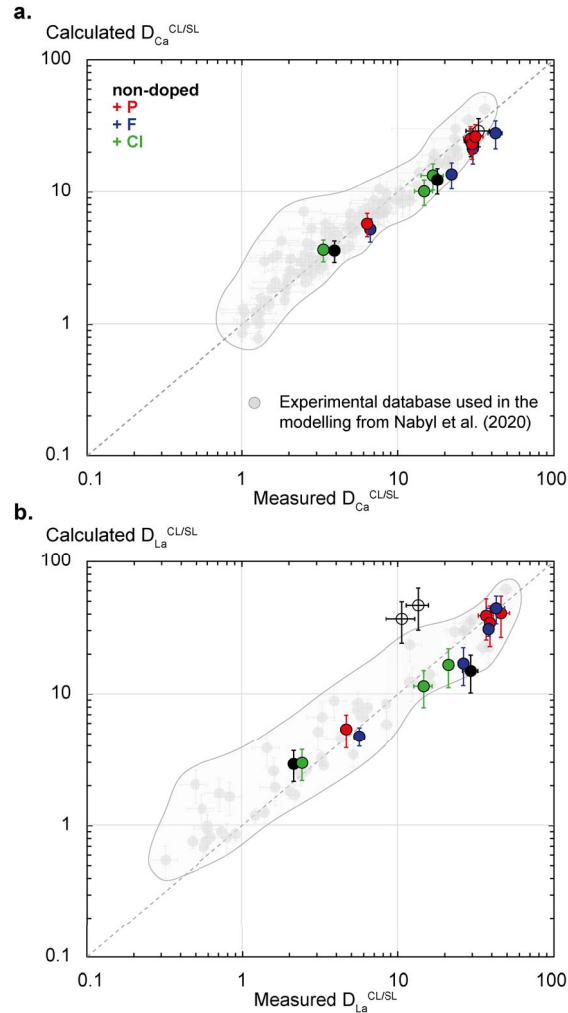


Figure 8. Application of the carbonate melt REE enrichment model from Nabyl *et al.* [2020] in the experimental F-Cl-P-rich carbonate and silicate liquids from this study. (a) Modelled Ca partition coefficients between carbonate and silicate liquids (Calculated $D_{Ca}^{CL/SL}$) versus the experimentally measured Ca partition coefficients (Measured $D_{Ca}^{CL/SL}$) from this study and the experimental database used for the Nabyl *et al.* [2020] model [Brooker, 1998, Freestone and Hamilton, 1980, Hamilton *et al.*, 1989, Jones *et al.*, 1995, Kjarsgaard, 1998, Kjarsgaard *et al.*, 1995, Martin *et al.*, 2013, 2012, Massuyeau *et al.*, 2015, Veksler *et al.*, 2012, 1998] (b) Modelled La partition coefficients between carbonate and silicate liquids (Calculated $D_{La}^{CL/SL}$) versus the experimentally measured La partition coefficients (Measured $D_{La}^{CL/SL}$) from this study and the experimental database [Hamilton *et al.*, 1989, Martin *et al.*, 2013, Veksler *et al.*, 2012]. All the samples synthesized in the four chemical systems (in black for the system with no additional volatile, red for the P-rich system, blue for the F-rich system and green for the Cl-rich system), at 850 °C–1050 °C–0.8 GPa and \pm additional H₂O are represented. The grey field corresponds to the experimental database used to calibrate the model from Nabyl *et al.* [2020]. Empty symbols correspond to samples suspected to not be in equilibrium (PCPC1_01 and PCPC1_02).

Veksler *et al.* [2012] have defined rare metal partitioning between salt melts—such as fluoride ($F > 38$ wt%), phosphate ($P_2O_5 > 45$ wt%) and chloride melts—and silicate melts. Fluoride and phosphate melts can be 100 times more enriched in REE than silicate melts [$D_{REE}^{Fluoride \text{ or Phosphate liquid/SL}} > 100$, Veksler *et al.*, 2012], which indicates a strong affinity for the salt melts. Figure 9 shows the La partition coefficients between fluoride/phosphate and silicate liquids versus the Ca partition coefficients from Veksler *et al.* [2012], compared to the samples from this study (carbonate and silicate liquids enriched \pm in F, Cl and P, see Figure 7). The same correlation between the La and the Ca partitioning is observed: the Ca-rich fluoride (blue empty triangle, Figure 9) and phosphate liquids (red empty triangle, Figure 9) are enriched in La ($D_{La}^{Fluoride \text{ or Phosphate liquid/SL}} > 100$). In other words, fluoride and phosphate liquids coexisting with Ca-poor silicate liquids are highly enriched in REE. This implies that the silicate melt composition and the structural effect governing REE partitioning in the carbonate–silicate liquid system [Figure 5; see Nabyl *et al.*, 2020] must also operate for REE partitioning between fluoride/phosphate and silicate liquids. As expected from the relationships between silicate melt polymerisation and REE partitioning, the silicate melts coexisting with salt melts from Veksler *et al.* [2012] have highly polymerised compositions (SiO_2 : 60 to 80 wt%; CaO: 0.03 to 7 wt%). Although these melts are not alkaline magmas, Figure 9 indicates that there is a seemingly universal trend linking Ca and REE partitioning between silicate and ionic melts.

4.3.2. Application to natural carbonate and silicate melt inclusions

Melt inclusion studies of alkaline magmatic rocks have highlighted the existence of inclusions containing alkaline silica–undersaturated silicate melts (melilitic to phonolitic compositions) coexisting with carbonate melts [Berkesi *et al.*, 2020, Guzmics *et al.*, 2012, 2019, Mitchell, 2009]. Guzmics *et al.* [2019] and Berkesi *et al.* [2020] have shown the existence of carbonate and silicate melt inclusions containing relatively high F, Cl and P concentrations, with up to 14 wt% of F, 5 wt% of P_2O_5 and 4 wt% of Cl in the carbonate melts. Those concentration ranges are similar to the melt concentrations reported in this study (see Table 3). The Nabyl *et al.* [2020] model (1) and (2)

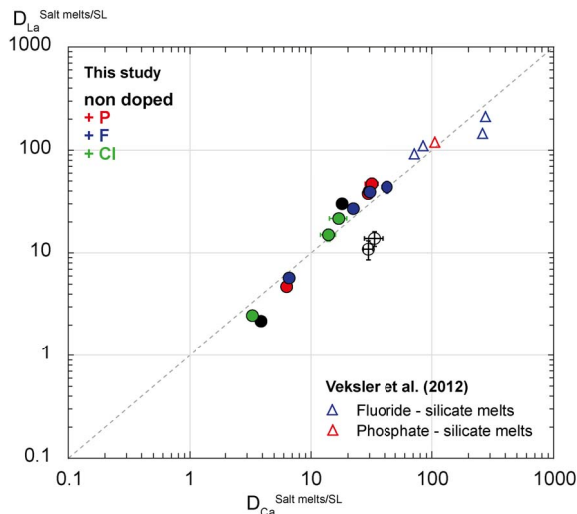


Figure 9. La partition ($D_{La}^{Salt \text{ melts/SL}}$) versus Ca partition coefficient ($D_{Ca}^{Salt \text{ melts/SL}}$) between carbonate melts from this study/salt melts from Veksler *et al.* [2012] and silicate liquids (Salt melts and SL). All samples from this study (samples synthesized in the four chemical systems: in black for the system with no additional volatile, red for the P-rich system, blue for the F-rich system and green for the Cl-rich system; at 850 °C–1050 °C–0.8 GPa; \pm additional H_2O) are compared to a sample in the fluoride–silicate liquid system [blue triangle, Veksler *et al.*, 2012] and one in the phosphate–silicate liquid system [red triangle, Veksler *et al.*, 2012].

has been applied to the conjugate carbonate and silicate melt inclusions, including in F-rich system. Only the $D_{Ca}^{CL/SL}$ has been modelled as the REE have not been analysed in the aforementioned melt inclusions studies; the calculated Ca partitioning are plotted against the measured ones in black in Figure 10 [Guzmics *et al.*, 2012, Mitchell, 2009], and in blue for F-rich melt inclusions [Berkesi *et al.*, 2020, Guzmics *et al.*, 2019]. For all melt inclusions, the $D_{Ca}^{CL/SL}$ in carbonate and silicate melts \pm rich in F, Cl and P are well reproduced by the modelling (Figure 10). This methodology can therefore be used as a test of equilibrium and a measure of the level of REE enrichment in carbonate melts during magmatic processes. For the cases illustrated in Figure 10, the $D_{Ca}^{CL/SL}$ values of around 20 imply $D_{La}^{CL/SL}$ values of around 30–40, in

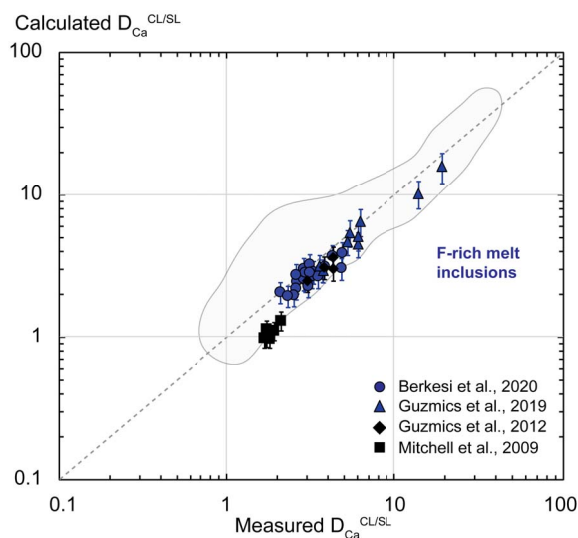


Figure 10. Application of the carbonate melt REE enrichment model from Nabyl *et al.* [2020] on natural carbonate and silicate melt inclusions. Modelled Ca partition coefficients between carbonate and silicate liquids (Calculated $D_{Ca}^{CL/SL}$) are shown together with measured Ca partition coefficients, for carbonate and silicate melt inclusions [in black; data from Mitchell, 2009, Guzmics *et al.*, 2012] and F-rich melt inclusions [in blue; data from Berkési *et al.*, 2020, Guzmics *et al.*, 2019]. The grey field corresponds to the experimental database used to calibrate the model from Nabyl *et al.* [2020].

other words the carbonatite melts must be strongly enriched in REE.

4.4. Role of the fluid phase

This section aims at highlighting a possible role of the fluid phase in REE behaviour between carbonate and alkaline silicate melts. As explained in Section 3.1, some charges present the texture of a fluid phase in contact with the carbonate and the silicate liquids (Figure 1d; Figures 2a, d and f; see Table 2), and the evidences presented above indicate its possible implication in Cl, alkali and REE behaviour.

The carbonate and silicate liquids in the Cl-rich system have low Cl concentrations (Cl < 1 wt%; samples PCPC5_02, PCPC5_03 and PCPC6_02; see Tables 2 and 3), despite the starting material contain-

ing 4.72 wt% of Cl (PhCbn 4, Table 1). The $D_{Cl}^{CL/SL}$ values of these samples are also relatively low (Figures 6c and d; Table 5). Apart from apatite, the other phases (clinopyroxene, garnet, and nepheline; see Table 2) at equilibrium with both liquids cannot concentrate Cl; still, only a few crystals of apatite have been observed in the charge (Figure 2g) and they do not explain such a Cl-loss during the experiment. It can therefore be assumed that Cl has been concentrated into the fluid phase during the experiments, especially in hydrated samples at 850 °C (3 and 6 wt% of H₂O, PCPC5_02 and PCPC5_03; see Table 2).

Moreover, the alkali content of carbonate melts decreases in the Cl-rich system with the addition of water (3 and 6 wt% of H₂O, samples PCPC5_02 and PCPC5_03, see Section 3.2 and Figure 3d). As the carbonate melts show a porous texture (Figures 1d and 2g), we can presume that Cl⁻ forms complexes with Na⁺ or K⁺ that concentrate into the fluid phase at equilibrium with other liquid and crystal phases. The addition of water increases the amount of fluid phase, which accordingly enhances the removal of Na, K and Cl from both melts. The fluid phase plays an important role in the carbonate melt composition in the Cl-rich system, therefore leading to a change in the concentrations of alkali elements in carbonate melts.

Furthermore, the carbonate melt REE concentrations are also slightly lower in the Cl-rich samples with additional water (PCPC5_02 and PCPC5_03, Table 4; see Section 3.3), whereas the silicate melt REE concentrations do not vary significantly (Table 4), apart from the Ce concentration as described above. This results in a decrease in $D_{REE}^{CL/SL}$ with the addition of water (Figure 4d). In fact, the REE have been shown to be mobile in aqueous fluids, especially in Cl- and F-rich fluids [Humphris and Henderson, 1984, Migdisov *et al.*, 2016, Williams-Jones *et al.*, 2012]. Migdisov *et al.* [2016] also characterised Cl as the principal agent of REE transport in aqueous fluids. We thus propose that REE also concentrate into the magmatic fluid phase in Cl-rich system, potentially creating complexes with Cl and alkali elements. In these samples, alkalis, Cl and REE seem to mainly interact in the fluid phase. This may well affect REE behaviour during the differentiation of alkaline/carbonatite systems, as well as REE ore forming processes [Gysi and Williams-Jones, 2015,

Smith *et al.*, 2016, Verplanck *et al.*, 2016, Williams-Jones *et al.*, 2012].

5. Conclusion

This study presents experiments on the REE partitioning between immiscible alkaline silicate melts of nephelinite–phonolite type and carbonate melts, for systems that are doped in F, Cl and P. The partitioning data for these doped systems are indistinguishable from those previously modelled by Nabyl *et al.* [2020] in F-, Cl- and P-poor systems. The Nabyl *et al.* [2020] REE partitioning model can therefore be applied on any system. We use this model on natural melt inclusions revealing carbonate–silicate pairs that can be used as a test of equilibrium and to predict the level of REE enrichment in the carbonatite melt. We suggest that Cl-rich systems tend to form magmatic fluids that are likely enriched in Na and REE. Further studies on the fluid phase are nevertheless necessary to link the magmatic processes and the late magmatic hydrothermal processes thought to be commonly involved in the formation of REE-rich deposits.

Conflicts of interest

Authors have no conflict of interest to declare.

Acknowledgements

This study was a part of Z. Nabyl's PhD, and was supported by the European Research Council (Grant no. 279790), the LABEX VOLTAIRE project (ANR-10-LABX-100-01) and the BRGM. Part of the experiments used was funded by the EquipEx PLANEX project (ANR-11-EQPX-0036). We thank J.-L. Devidal from the LMV laboratory (Laboratoire Magmas et Volcans, Clermont-Ferrand, France) and S. Erdmann from the ISTO laboratory (Orléans, France) for their support with LA-ICP-MS analysis and data treatment. We are grateful to two anonymous reviewers for their constructive comments and thoughtful advices on this manuscript.

Supplementary data

Supporting information for this article is available on the journal's website under <https://doi.org/10.5802/crgeos.104> or from the author.

References

- Ablay, G. J., Carroll, M. R., Palmer, M. R., Martí, J., and Sparks, R. S. J. (1998). Basanite–phonolite lineages of the teide–pico viejo volcanic complex, tenerife, canary islands. *J. Petrol.*, 39, 905–936.
- Adachi, G. and Imanaka, N. (1998). The binary rare earth oxides. *Chem. Rev.*, 98, 1479–1514.
- Aiuppa, A., Baker, D. R., and Webster, J. D. (2009). Halogens in volcanic systems. *Chem. Geol.*, 263, 1–18. Special Issue: Halogens in Volcanic Systems and Their Environmental Impacts.
- Anenburg, M., Mavrogenes, J. A., Frigo, C., and Wall, F. (2020). Rare earth element mobility in and around carbonatites controlled by sodium, potassium, and silica. *Sci. Adv.*, 6, article no. eabb6570.
- Baasner, A., Schmidt, B. C., Dupree, R., and Webb, S. L. (2014). Fluorine speciation as a function of composition in peralkaline and peraluminous Na₂O–CaO–Al₂O₃–SiO₂ glasses: A multinuclear NMR study. *Geochim. Cosmochim. Acta*, 132, 151–169.
- Baasner, A., Schmidt, B. C., and Webb, S. L. (2013a). The effect of chlorine, fluorine and water on the viscosity of aluminosilicate melts. *Chem. Geol.*, 357, 134–149.
- Baasner, A., Schmidt, B. C., and Webb, S. L. (2013b). Compositional dependence of the rheology of halogen (F, Cl) bearing aluminosilicate melts. *Chem. Geol.*, 346, 172–183. Special Issue: 9th Silicate Melts Workshop.
- Baudouin, C., Parat, F., Denis, C. M. M., and Mangasini, F. (2016). Nephelinite lavas at early stage of rift initiation (Hanang volcano, North Tanzanian Divergence). *Contrib. Mineral. Petrol.*, 171, article no. 64.
- Baudouin, C., Parat, F., and Michel, T. (2018). CO₂-rich phonolitic melt and carbonatite immiscibility in early stage of rifting: Melt inclusions from Hanang volcano (Tanzania). *J. Volcanol. Geotherm. Res.*, 358, 261–272.
- Berkesi, M., Bali, E., Bodnar, R. J., Szabó, A., and Guzmics, T. (2020). Carbonatite and highly peralkaline nephelinite melts from Oldoinyo Lengai Volcano, Tanzania: The role of natrite–normative fluid degassing. *Gondwana Res.*, 85, 76–83.
- Brooker, R. A. (1998). The effect of CO₂ saturation on immiscibility between silicate and carbonate

- liquids: an experimental study. *J. Petrol.*, 39, 1905–1915.
- Brooker, R. A. and Kjarsgaard, B. A. (2011). Silicate-carbonate liquid immiscibility and phase relations in the system $\text{SiO}_2\text{-Na}_2\text{O-Al}_2\text{O}_3\text{-CaO-CO}_2$ at 0.1–2.5 GPa with applications to carbonatite genesis. *J. Petrol.*, 52, 1281–1305.
- Burnham, A. D. and Berry, A. J. (2014). The effect of oxygen fugacity, melt composition, temperature and pressure on the oxidation state of cerium in silicate melts. *Chem. Geol.*, 366, 52–60.
- Castor, S. B. (2008). The Mountain Pass rare-earth carbonatite and associated ultrapotassic rocks, California. *Can. Mineral.*, 46, 779–806.
- Chakhmouradian, A. R. and Zaitsev, A. N. (2012). Rare earth mineralization in igneous rocks: sources and processes. *Elements*, 8, 347–353.
- Chebotarev, D. A., Veksler, I. V., Wohlgemuth-Ueberwasser, C., Doroshkevich, A. G., and Koch-Müller, M. (2019). Experimental study of trace element distribution between calcite, fluorite and carbonatitic melt in the system $\text{CaCO}_3 + \text{CaF}_2 + \text{Na}_2\text{CO}_3 \pm \text{Ca}_3(\text{PO}_4)_2$ at 100 MPa. *Contrib. Mineral. Petrol.*, 174, article no. 4.
- Dasgupta, R., Hirschmann, M. M., and Withers, A. C. (2004). Deep global cycling of carbon constrained by the solidus of anhydrous, carbonated eclogite under upper mantle conditions. *Earth Planet. Sci. Lett.*, 227, 73–85.
- Dawson, J. B. (1962). Sodium carbonate lavas from Oldoinyo Lengai, Tanganyika. *Nature*, 195, 1075–1076.
- Dingwell, D. B. (1986). Volatile solubilities in silicate melts. In *Silicate Melts: Their Properties and Structure Applied to Problems in Geochemistry, Petrology, Economic Geology, and Planetary Geology*, pages 93–129. Mineralogical Association of Canada, Québec, Canada.
- Feng, M., Song, W., Kynicky, J., Smith, M., Cox, C., Kotlanova, M., Brtnicky, M., Fu, W., and Wei, C. (2020). Primary rare earth element enrichment in carbonatites: Evidence from melt inclusions in Ulgii Khiid carbonatite, Mongolia. *Ore Geol. Rev.*, 117, article no. 103294.
- Freestone, I. C. and Hamilton, D. L. (1980). The role of liquid immiscibility in the genesis of carbonatites—an experimental study. *Contrib. Mineral. Petrol.*, 73, 105–117.
- Frezzotti, M.-L. (2001). Silicate-melt inclusions in magmatic rocks: applications to petrology. *Lithos*, 55, 273–299. Special Issue: Fluid Inclusions: Phase Relationships - Methods - Applications. A Special Issue in honour of Jacques Touret.
- Guzmics, T., Berkesi, M., Bodnar, R. J., Fall, A., Bali, E., Milke, R., Vetlényi, E., and Szabó, C. (2019). Natro-carbonatites: A hidden product of three-phase immiscibility. *Geology*, 47, 527–530.
- Guzmics, T., Mitchell, R. H., Szabó, C., Berkesi, M., Milke, R., and Ratter, K. (2012). Liquid immiscibility between silicate, carbonate and sulfide melts in melt inclusions hosted in co-precipitated minerals from Kerimasi volcano (Tanzania): evolution of carbonated nephelinitic magma. *Contrib. Mineral. Petrol.*, 164, 101–122.
- Gysi, A. P. and Williams-Jones, A. E. (2015). The thermodynamic properties of bastnäsite-(Ce) and parisite-(Ce). *Chem. Geol.*, 392, 87–101.
- Hamilton, D. L., Bedson, P., and Esson, J. (1989). The behaviour of trace elements in the evolution of carbonatites. In Bell, K., editor, *Carbonatites, Genesis and Evolution*, pages 405–427. Unwin-Hyman, London, UK.
- Humphris, S. E. and Henderson, P. (1984). The mobility of the rare earth elements in the crust. *Rare Earth Element Geochem.*, 2, 317–342.
- Jago, B. C. and Gittins, J. (1991). The role of fluorine in carbonatite magma evolution. *Nature*, 349, 56–58.
- Jia, Y. and Liu, Y. (2020). REE enrichment during magmatic-hydrothermal processes in carbonatite-related REE deposits: A case study of the Weishan REE deposit, China. *Minerals*, 10, article no. 25.
- Jochum, K. P., Weis, U., Schwager, B., Stoll, B., Wilson, S. A., Haug, G. H., Andreae, M. O., and Enzweiler, J. (2016). Reference values following ISO guidelines for frequently requested rock reference materials. *Geostand. Geoanalytical Res.*, 40, 333–350.
- Jones, A. P., Genge, M., and Carmody, L. (2013). Carbonate melts and carbonatites. *Rev. Mineral. Geochem.*, 75, 289–322.
- Jones, J. H., Walker, D., Pickett, D. A., Murrell, M. T., and Beattie, P. (1995). Experimental investigations of the partitioning of Nb, Mo, Ba, Ce, Pb, Ra, Th, Pa, and U between immiscible carbonate and silicate liquids. *Geochim. Cosmochim. Acta*, 59, 1307–1320.
- Keller, J. and Zaitsev, A. N. (2012). Geochemistry and petrogenetic significance of natrocarbonatites at

- Oldoinyo Lengai, Tanzania: Composition of lavas from 1988 to 2007. *Lithos*, 148, 45–53.
- Kjarsgaard, B. A. (1998). Phase relations of a carbonated high-CaO nephelinite at 0.2 and 0.5 GPa. *J. Petrol.*, 39, 2061–2075.
- Kjarsgaard, B. A. and Hamilton, D. L. (1988). Liquid immiscibility and the origin of alkali-poor carbonatites. *Mineral. Mag.*, 52, 43–55.
- Kjarsgaard, B. A., Hamilton, D. L., and Peterson, T. D. (1995). Peralkaline nephelinite/carbonatite liquid immiscibility: comparison of phase compositions in experiments and natural lavas from Oldoinyo Lengai. In *Carbonatite Volcanism Oldoinyo Lengai and the Petrogenesis of Natrocarbonatite, IAVCEI Proceedings in Volcanology*, pages 163–190. Springer, Berlin, Heidelberg.
- Kynicky, J., Smith, M. P., Song, W., Chakhmouradian, A. R., Xu, C., Kopriva, A., Galiova, M. V., and Brtnicky, M. (2019). The role of carbonate-fluoride melt immiscibility in shallow REE deposit evolution. *Geosci. Front. Clim. Change Impacts Environ. Geosci.*, 10, 527–537.
- Lee, W. and Wyllie, P. J. (1994). Experimental data bearing on liquid immiscibility, crystal fractionation, and the origin of calciocarbonatites and natrocarbonatites. *Int. Geol. Rev.*, 36, 797–819.
- Louvel, M., Bordage, A., Testemale, D., Zhou, L., and Mavrogenes, J. (2015). Hydrothermal controls on the genesis of REE deposits: Insights from an in situ XAS study of Yb solubility and speciation in high temperature fluids ($T < 400$ °C). *Chem. Geol.*, 417, 228–237.
- Mangler, M. F., Marks, M. A. W., Zaitzev, A. N., Eby, G. N., and Markl, G. (2014). Halogens (F, Cl and Br) at Oldoinyo Lengai volcano (Tanzania): Effects of magmatic differentiation, silicate–natrocarbonatite melt separation and surface alteration of natrocarbonatite. *Chem. Geol.*, 365, 43–53.
- Mariano, A. N. and Mariano, A. (2012). Rare earth mining and exploration in North America. *Elements*, 8, 369–376.
- Martin, L. H. J., Schmidt, M. W., Mattsson, H. B., and Guenther, D. (2013). Element partitioning between immiscible carbonatite and silicate melts for dry and H₂O-bearing systems at 1–3 GPa. *J. Petrol.*, 54, 2301–2338.
- Martin, L. H. J., Schmidt, M. W., Mattsson, H. B., Ulmer, P., Hametner, K., and Günther, D. (2012). Element partitioning between immiscible carbonatite–kamafugite melts with application to the Italian ultrapotassic suite. *Chem. Geol.*, 320–321, 96–112.
- Massuyeau, M., Gardés, E., Morizet, Y., and Gaillard, F. (2015). A model for the activity of silica along the carbonatite–kimberlite–mellilitite–basanite melt compositional joint. *Chem. Geol.*, 418, 206–216.
- Mattsson, H. B., Nandedkar, R. H., and Ulmer, P. (2013). Petrogenesis of the melilititic and nephelinitic rock suites in the Lake Natron–Engaruka monogenetic volcanic field, northern Tanzania. *Lithos*, 179, 175–192.
- Metrich, N. and Rutherford, M. J. (1992). Experimental study of chlorine behavior in hydrous silicic melts. *Geochim. Cosmochim. Acta*, 56, 607–616.
- Migdisov, A., Williams-Jones, A. E., Brugger, J., and Caporuscio, F. A. (2016). Hydrothermal transport, deposition, and fractionation of the REE: Experimental data and thermodynamic calculations. *Chem. Geol.*, 439, 13–42.
- Mitchell, R. H. (2005). Carbonatites and carbonatites and carbonatites. *Can. Mineral.*, 43, 2049–2068.
- Mitchell, R. H. (2009). Peralkaline nephelinite–natrocarbonatite immiscibility and carbonatite assimilation at Oldoinyo Lengai, Tanzania. *Contrib. Mineral. Petrol.*, 158, article no. 589.
- Mysen, B. O. (1998). Phosphorus solubility mechanisms in haplogranitic aluminosilicate glass and melt: effect of temperature and aluminum content. *Contrib. Mineral. Petrol.*, 133, 38–50.
- Mysen, B. O., Ryerson, F. J., and Virgo, D. (1981). The structural role of phosphorus in silicate melts. *Am. Mineral.*, 66, 106–117.
- Mysen, B. O., Virgo, D., and Seifert, F. A. (1982). The structure of silicate melts: Implications for chemical and physical properties of natural magma. *Rev. Geophys.*, 20, 353–383.
- Nabyl, Z., Massuyeau, M., Gaillard, F., Tuduri, J., Iacono-Marziano, G., Rogerie, G., Le Trong, E., Di Carlo, I., Melleton, J., and Bailly, L. (2020). A window in the course of alkaline magma differentiation conducive to immiscible REE-rich carbonatites. *Geochim. Cosmochim. Acta*, 282, 297–323.
- Nelson, D. R., Chivas, A. R., Chappell, B. W., and McCulloch, M. T. (1988). Geochemical and isotopic systematics in carbonatites and implications for the evolution of ocean-island sources. *Geochim.*

- Cosmochim. Acta*, 52, 1–17.
- Néron, A., Bédard, L. P., and Gaboury, D. (2018). The saint-honoré carbonatite REE Zone, Québec, Canada: combined magmatic and hydrothermal processes. *Minerals*, 8, article no. 397.
- Panina, L. I. (2005). Multiphase carbonate-salt immiscibility in carbonatite melts: data on melt inclusions from the Krestovskiy massif minerals (Polar Siberia). *Contrib. Mineral. Petrol.*, 150, 19–36.
- Panina, L. I. and Motorina, I. V. (2008). Liquid immiscibility in deep-seated magmas and the generation of carbonatite melts. *Geochem. Int.*, 46, 448–464.
- Pearce, N. J. G., Perkins William, T., Westgate John, A., Gorton Michael, P., Jackson Simon, E., Neal Clive, R., and Chenery Simon, P. (1997). A compilation of new and published major and trace element data for NIST SRM 610 and NIST SRM 612 glass reference materials. *Geostand. Newsl.*, 21, 115–144.
- Ponader, C. W. and Brown, G. E. (1989). Rare earth elements in silicate glassmelt systems: II. Interactions of La, Gd, and Yb with halogens. *Geochim. Cosmochim. Acta*, 53, 2905–2914.
- Potter, N. J., Kamenetsky, V. S., Simonetti, A., and Goemann, K. (2017). Different types of liquid immiscibility in carbonatite magmas: A case study of the Oldoinyo Lengai 1993 lava and melt inclusions. *Chem. Geol.*, 455, 376–384. Special Issue: The Role of Intraplate Magmas and their Inclusions in Earth's Mantle Evolution.
- Rocholl, A. (1998). Major and trace element composition and homogeneity of microbeam reference material: basalt glass USGS BCR-2G. *Geostand. Newsl.*, 22, 33–45.
- Schaller, T., Dingwell, D. B., Keppler, H., Knöller, W., Merwin, L., and Sebald, A. (1992). Fluorine in silicate glasses: A multinuclear nuclear magnetic resonance study. *Geochim. Cosmochim. Acta*, 56, 701–707.
- Sifré, D., Gardés, E., Massuyeau, M., Hashim, L., Hier-Majumder, S., and Gaillard, F. (2014). Electrical conductivity during incipient melting in the oceanic low-velocity zone. *Nature*, 509, 81–85.
- Smith, M. P., Moore, K., Kavecsánszki, D., Finch, A. A., Kynicky, J., and Wall, F. (2016). From mantle to critical zone: a review of large and giant sized deposits of the rare earth elements. *Geosci. Front.*, 7, 315–334. Special Issue: Giant Mineral Deposits.
- Stagno, V. and Frost, D. J. (2010). Carbon speciation in the asthenosphere: Experimental measurements of the redox conditions at which carbonate-bearing melts coexist with graphite or diamond in peridotite assemblages. *Earth Planet. Sci. Lett.*, 300, 72–84.
- Toplis, M. J. and Dingwell, D. B. (1996). The variable influence of P₂O₅ on the viscosity of melts of differing alkali/aluminium ratio: Implications for the structural role of phosphorus in silicate melts. *Geochim. Cosmochim. Acta*, 60, 4107–4121.
- Van Achterbergh, E., Ryan, C., and Griffin, W. (2001). GLITTER user's manual: on-line interactive data reduction for the LA-ICP-MS microprobe. Version 4.
- Veksler, I. V., Dorfman, A. M., Dulski, P., Kamenetsky, V. S., Danyushevsky, L. V., Jeffries, T., and Dingwell, D. B. (2012). Partitioning of elements between silicate melt and immiscible fluoride, chloride, carbonate, phosphate and sulfate melts, with implications to the origin of natrocarbonatite. *Geochim. Cosmochim. Acta*, 79, 20–40.
- Veksler, I. V., Dorfman, A. M., Kamenetsky, M., Dulski, P., and Dingwell, D. B. (2005). Partitioning of lanthanides and Y between immiscible silicate and fluoride melts, fluorite and cryolite and the origin of the lanthanide tetrad effect in igneous rocks. *Geochim. Cosmochim. Acta*, 69, 2847–2860.
- Veksler, I. V., Petibon, C., Jenner, G. A., Dorfman, A. M., and Dingwell, D. B. (1998). Trace element partitioning in immiscible silicate-carbonate liquid systems: an initial experimental study using a centrifuge autoclave. *J. Petrol.*, 39, 2095–2104.
- Verplanck, P. L., Mariano, A. N., and Mariano Jr., A. (2016). Rare earth element ore geology of carbonatites. *Rev. Econ. Geol.*, 18, 5–32.
- Wall, F. and Mariano, A. (1996). Rare earth minerals in carbonatites: a discussion centred on the Kangankunde Carbonatite, Malawi. In Jones, A. P., Wall, F., and Williams, C. T., editors, *Rare Earth Minerals, Chemistry, Origin and Ore Deposits*, Mineralogical Society Series, pages 193–226. Chapman & Hall, London, UK.
- Webster, J. D., Baker, D. R., and Aiuppa, A. (2018). Halogens in mafic and intermediate-silica content magmas. In Harlov, D. E. and Aranovich, L., editors, *The Role of Halogens in Terrestrial and Extraterrestrial Geochemical Processes: Surface, Crust, and Mantle*, Springer Geochemistry, pages 307–430. Springer International Publishing, Cham, Switzerland.

- Williams-Jones, A. E., Migdisov, A. A., and Samson, I. M. (2012). Hydrothermal mobilisation of the rare earth elements—a tale of “Ceria” and “Yttria”. *Elements*, 8, 355–360.
- Woolley, A. R. and Kempe, D. R. C. (1989). Carbonatites: nomenclature, average chemical compositions, and element distribution. In Bell, K., editor, *Carbonatites, Genesis and Evolution*, pages 1–14. Unwin-Hyman, London, UK.
- Woolley, A. R. and Kjarsgaard, B. A. (2008). Paragenetic types of carbonatite as indicated by the diversity and relative abundances of associated silicate rocks: evidence from a global database. *Can. Mineral.*, 46, 741–752.